IEEE Access
Multidisciplinary ⋮ Rapid Review ⋮ Open Access Journal

Received October 18, 2020, accepted November 16, 2020, date of publication November 18, 2020,
date of current version December 7, 2020.

Digital Object Identifier 10.1109/ACCESS.2020.3039001

Global Asymptotic Nonlinear PID Control With a New Generalized Saturation Function

GUOJUN NIU[1] AND CUICUI QU[2]
[1]School of Mechanical Engineering and Automation, Zhejiang Sci-Tech University, Hangzhou 310018, China
[2]Hangzhou SIASUN Robot and Automation Company Ltd., Hangzhou 311200, China

Corresponding author: Guojun Niu (niuguojun@zstu.edu.cn)

This work was supported in part by the National Natural Science Foundation of China under Grant 61803341, in part by the Natural Science Foundation of Zhejiang Province under Grant LY20E050019, and in part by the State Key Laboratory of Robotics and System [Harbin Institute of Technology (HIT)] under Grant SKLRS-2019-KF-08.

ABSTRACT In order to solve the problem of the strict condition of traditional saturation function, a new generalized saturation function was proposed and applied in nonlinear PID (Proportion-Integration-Differentiation) control laws, which consisted of linear D + nonlinear PI and linear PD + nonlinear PI. The new generalized saturation function has powerful reaction near the equilibrium point, and has the capability to make the control converge to the equilibrium point swiftly. The global asymptotic stability condition of nonlinear PID control laws were derived by employing Lyapunov's method and LaSalle's invariance principle. In order to improve the accuracy of nonlinear PID control laws, time integration of the absolute value of position tracking error and time integration of the absolute value of torque error were chosen as the objective functions. Global asymptotic stability conditions and rated driving torque of each motor were set as the constraint conditions. Nonlinear PID controller parameters were tuned by employing multi-objective genetic algorithm, non-dominated sorted genetic algorithm-II (NSGA-II). Compared with the optimization results of nonlinear PID with traditional saturation function, the accuracy of position tracking using the proposed method was improved by nearly one order of magnitude. The new generalized saturation functions with minimum time integration of position tracking error were selected to study the robustness of the nonlinear PID controller in modeling uncertainty, input torque disturbance, and noise. The position tracking accuracy of the proposed method compared to those of the traditional PID controller and nonlinear PID controller with traditional saturation function was improved by nearly two orders of magnitude and one order of magnitude, respectively. The introduced saturation function significantly improves position tracking accuracy and robustness of the nonlinear PID controller.

INDEX TERMS Nonlinear PID, saturation function, global asymptotic stability, robust.

I. INTRODUCTION

In recent years, many complex control strategies have been proposed in the literature. However, PID control is still widely employed in actual robot control because of its simple structure, small amount of calculation, and good real-time performance [1]. Classical linear PID controllers do not demonstrate global stability. Enhanced versions of PID controllers, by applying nonlinear saturation function, have been put forward to ensure global stability. Alvarez-Ramirez proved the semi-global stability of saturated linear PID when there were adequate large proportional, enough small integral, and torque bounds larger than gravitational torques [2], [3]. Ortega proposed a semi-globally stable output-feedback PI^2D regulator, where the main contribution was to avoid the need for gravity forces information via the inclusion of two integral terms around the position error, and the filtered position [4]. In addition, Liu introduced a semi-globally stable PD-I(PD) regulator [5]. Nonlinear saturation functions were not in the above semi-globally stable PID controllers. PD control law along with a class of nonlinear integral actions, proposed by Kelly, was globally asymptotically stable [6]. Gorez introduced PID-like control to achieve global asymptotic stability (GAS) of the desired steady state configuration of mechanical system with actuator constraints [7]. Globally stabilizing PID-type control scheme with a generalized

The associate editor coordinating the review of this manuscript and approving it for publication was Azwirman Gusrialdi.

saturating structure and constrained inputs was proposed by Mendoza *et al.* [8], [9]. Santibanez proposed a saturated nonlinear PID control for industrial robot manipulators by taking the natural saturation problem into consideration [10]. Furthermore, Zavalario proposed a natural saturated extension of PD with desired gravity compensation control law and constrained input that was globally asymptotically stable [11], [12]. Then, an output-feedback PID with multiple saturating structures and constrained inputs guaranteed the global stability [13]. Salinas put forward a family of locally asymptotically stable nonlinear PID control law, where stability conditions were independent of the saturation levels of actuators [14]. In addition, Yarza introduced a nonlinear PID controller with bounded torques using a single saturation function that was globally asymptotically stable [15]. Liu proposed a set of globally stable output-feedback N-PID control laws that were dealing with the position control problem of designing asymptotically stable proportional plus integral regulators with only position feedback [16]. A saturated PID control was raised to address the global asymptotic regulation of robot under input constraints, both with and without velocity measurement by Su [17]. In order to ensure the stability of the PID control laws, there are nonlinear saturation terms. However, definition of the saturation function is strict. In this study, a new generalized saturation function with smaller constraints is proposed, and can be used to prove the stability of nonlinear PID control law. At the same time, the generalized saturation function is useful in improving the precision of the PID control law.

PID parameters tuning affects the accuracy of PID control law. Killingsworth proposed extremum seeking for tuning PID controllers by minimizing a cost function characterizing the desired behavior of the closed-loop system; however, extremum seeking required initial values [18]. Duan put forward the ant colony algorithm to tune nonlinear PID parameters [19]. Li raised a robust PID tuning method based on nonlinear optimization with specified gain and phase margins [20]. A multi-crossover genetic approach for tuning multivariable PID controllers was proposed by Chang [21]. Multi-objective PID parameters tuning for a flexible AC transmission system (FACTS)-based damping stabilizer using NSGA-II was raised by Panda [22]. A tuning method based on fruit fly optimization algorithm was proposed to optimize PID controller parameters by Han *et al.* [23]. Also, Sun proposed a PID parameters tuning strategy based on dynamic stiffness for the radial active magnetic bearing [24]. Further, Khodja used particle swarm optimization to tune PID attitude stabilization of a quadrotor [25]. Leva raised the explicit model-based real PID tuning for efficient load disturbance rejection [26]. A mean for PID tuning based on the neutrosophic similarity measure was introduced by Can and Ozguven [27]. Interactive tool for frequency domain tuning of PID controllers was put forward by Garrido *et al.* [28]. A practical interactive PID tuning method for mechanical systems using parameter chart was proposed by Kang *et al.* [29]. In summary, the intelligent optimization algorithms were utilized to tuning PID parameters. However, GAS constraints are not taken into account in PID parameter tuning. In this research work, under the constraint of GAS and rated driving torque of each motor, the time integration of the absolute value of position tracking error and time integration of the absolute value of input torque error are chosen as the objective functions and NSGA-II is employed to realize the tuning of global asymptotic stable PID parameters.

The report is organized as follows: Section II introduces preliminaries. Section III solves stability analysis of nonlinear PID control. Parameters tuning of nonlinear PID control laws are presented in Section IV. Section V. discusses the robustness analysis of nonlinear PID. Finally, Section VI concludes the paper.

II. PRELIMINARIES

A. DEFINITION OF A NEW SATURATION FUNCTION

Definition 1 [30] Given positive constants L and M, with L<M, a function $\boldsymbol{\sigma}(x; \mathrm{L}, \mathrm{M})$: R→R: $x \mapsto \boldsymbol{\sigma}(x; \mathrm{L}, \mathrm{M})$ is said to be a linear saturation function if $\boldsymbol{\sigma}(x; \mathrm{L}, \mathrm{M})$ is continuously non-monotone decreasing and satisfies (1). $\boldsymbol{\sigma}(x; \mathrm{L}, \mathrm{M})$ is said to be a simple linear saturation function if $\boldsymbol{\sigma}(x; \mathrm{L}, \mathrm{M})$ satisfies (2).

$$\begin{aligned} &(1)\, x\sigma(x) > 0 \text{ when } x \neq 0; \\ &(2)\, \sigma(x) = x \text{ when } |x| \leq \mathrm{L}; \\ &(3)\, |\sigma(x)| \leq \mathrm{M} \text{ when } x \in \mathrm{R} \end{aligned} \tag{1}$$

$$\begin{aligned} &(1)\, x\sigma(x) > 0 \text{ when } x \neq 0; \\ &(2)\, \sigma(x) = x \text{ when } |x| \leq \mathrm{L}; \\ &(3)\, |\sigma(x)| = M \text{ when } |x| \geq \mathrm{M} \end{aligned} \tag{2}$$

Definition 2 [6]: Given positive constants α and β, with $0 < \alpha \leq 1, \boldsymbol{f}(\boldsymbol{x}) = [f(x_1) f(x_2) \cdots f(x_n)]^{\mathrm{T}}$, when $x \in \mathrm{R}^n$, a function $\boldsymbol{f}(x) : \mathrm{R} \to \mathrm{R}: x \mapsto \boldsymbol{f}(x)$ is said to be a saturation function if $f(x)$ is a continuously differentiable function and satisfies:

$$\begin{aligned} &(1)\ |x| \geq |f(x)| \geq \alpha |x|, \quad \forall x \in \mathrm{R} : |x| < \beta; \\ &(2)\ \beta \geq |f(x)| \geq \alpha\beta, \quad \forall x \in \mathrm{R} : |x| \geq \beta; \\ &(3)\ 1 \geq \left(df(x)/dx\right) \geq 0 \end{aligned} \tag{3}$$

Definition 3 [12]: Given positive constant F, a function $\delta(x)$: R→R: $x \mapsto \delta(x)$ is said to be a bounded generalized saturation function if $\delta(x)$ is a continuous monotone increasing function and satisfies:

$$\begin{aligned} &(1)\ x\delta(x) > 0 \text{ when } x \neq 0,\ x \in \mathrm{R}; \\ &(2)\ |\delta(x)| \leq \mathrm{F} \text{ when } x \in \mathrm{R} \end{aligned} \tag{4}$$

The definition 1, 2, and 3 can be summarized as: Given positive constant M_1, a function $\delta_1(x) : \mathrm{R} \to \mathrm{R}: x \mapsto \delta_1(x)$ is said to be a generalized saturation function if $\delta_1(x)$ is a continuously differentiable function and satisfies:

$$\begin{aligned} &(1)\ x\delta_1(x) > 0 \text{ when } x \neq 0,\ x \in \mathrm{R}; \\ &(2)\ |\delta_1(x)| \leq \mathrm{M}_1 \text{ when } x \in \mathrm{R} \end{aligned} \tag{5}$$

$\boldsymbol{\Gamma}_2(\boldsymbol{x})$ ($\boldsymbol{x} \in \mathrm{R}^n$) denotes the set of all continuously differentiable functions: $\Gamma_2(\boldsymbol{x}) = [\delta_1(x_1)\delta_1(x_2) \cdots \delta_1(x_n)]^{\mathrm{T}}$.

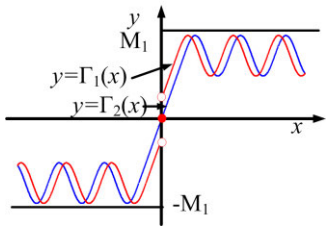

FIGURE 1. The difference between the generalized saturation $y = \Gamma_2(x)$ and the new generalized saturation $y = \Gamma_1(x)$.

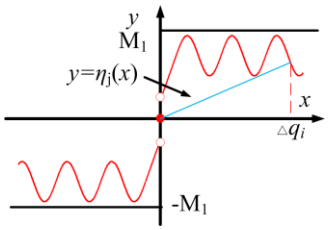

FIGURE 2. The new generalized saturated function $y = \Gamma 1(x)$.

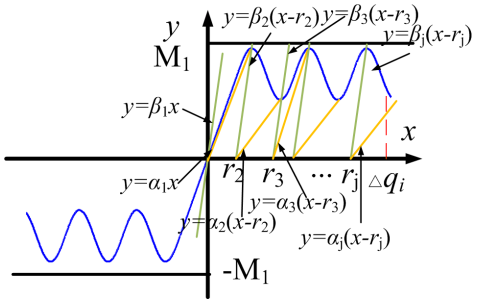

FIGURE 3. The saturated function $y = \Gamma 2(x)$.

The above saturation function definition conditions are more rigorous. A new generation of saturation function is given as follows:

Definition 4: Given a positive constant M_1, a function $\delta_2(x)$: R→R: $x \mapsto \delta_2(x)$ is said to be a new generalized saturation function if $\delta_2(x)$ is a bound function with only point ξ, $\delta_2(\xi) = 0$ and satisfies:

$$\begin{aligned} &(1)\ x\delta_2(x) > 0 \text{ when } x \neq 0,\ x \in R; \\ &(2)\ |\delta_2(x)| \leq M_1 \text{ when } x \in R \end{aligned} \tag{6}$$

$\boldsymbol{\Gamma}_1(\boldsymbol{x})$ ($\boldsymbol{x} \in R^n$) denotes the set of all functions: $\boldsymbol{\Gamma}_1(\boldsymbol{x}) = [\delta_2(x_1)\delta_2(x_2)\cdots\delta_2(x_n)]^T$.

The definition 4 of the generalized saturation function consists of definitions 1, 2, and 3 of saturation functions. Definitions 1, 2, and 3 of saturation functions are special forms of definition 4 when the coefficient of sign function is zero. The functions $y = \Gamma_1(x)$ and $y = \Gamma_2(x)$ are shown in Figure 1. The relationship between $y = \Gamma_1(\boldsymbol{x})$ and $y = \Gamma_2(\boldsymbol{x})$ can be expressed as $\Gamma_1(\boldsymbol{x}) = \Gamma_2(x + \mu \text{sign}(x))$. Compared with definitions 1, 2, and 3 of saturation function, the new definition of saturation function has a strong reaction near the equilibrium point and the error can converge to the equilibrium point faster, under the PID control law.

B. PROBLEM FORMULATION

The dynamic system of an n-link rigid robot manipulator system [31] can be written as

$$\boldsymbol{M}(\boldsymbol{q})\ddot{\boldsymbol{q}} + \boldsymbol{C}(\boldsymbol{q}, \dot{\boldsymbol{q}})\dot{\boldsymbol{q}} + \boldsymbol{D}\dot{\boldsymbol{q}} + \boldsymbol{g}(\boldsymbol{q}) = \boldsymbol{\tau} \tag{7}$$

where $\boldsymbol{q},\ \dot{\boldsymbol{q}},\ \ddot{\boldsymbol{q}} \in R^n$ is $n\times1$ vector of joint displacements, velocity, and acceleration, $\tau \in R^n$ is $n\times1$ vector of applied joint torques, $\boldsymbol{M}(\boldsymbol{q})$ is $n \times n$ symmetric positive inertia matrix, $\boldsymbol{C}(\boldsymbol{q}, \dot{\boldsymbol{q}})$ is the $n\times n$ matrix of centripetal and coriolis torques, $\boldsymbol{D}$ is the $n \times n$ positive define diagonal friction matrix, $\boldsymbol{g}(\boldsymbol{q})$ is $n\times1$ vector of gravitational torques.

Property 1: The inertia matrix $\boldsymbol{M}(\boldsymbol{q})$ is a symmetric positive definite matrix.

Property 2: $\dot{\boldsymbol{q}}^T\left[0.5\dot{\boldsymbol{M}}(\boldsymbol{q}) - \boldsymbol{C}(\boldsymbol{q}, \dot{\boldsymbol{q}})\right]\dot{\boldsymbol{q}} = 0$, for all $\boldsymbol{q},\ \dot{\boldsymbol{q}} \in R^n$ and $\dot{\boldsymbol{M}}(\boldsymbol{q}) = \boldsymbol{C}(\boldsymbol{q}, \dot{\boldsymbol{q}}) + \boldsymbol{C}(\boldsymbol{q}, \dot{\boldsymbol{q}})^T$.

Property 3: There exists a positive constant k_{C1} such that $\|\boldsymbol{C}(\boldsymbol{q},\ \boldsymbol{x})\boldsymbol{y}\| \leq k_{C1}\|\boldsymbol{x}\|\|\boldsymbol{y}\|\ \forall \boldsymbol{q},\ \boldsymbol{x},\ \boldsymbol{y} \in R^n$.

In order to facilitate subsequent proof, the integrals of $y = \Gamma_1(x)$ and $y = \Gamma_2(x)$ are studied. When $x \in [0, \Delta q_i]$, $\Gamma_1(x)$ $\geq \eta_i x$, $\eta_i \in (0, \Gamma_1(x)/\Delta q_i)$, η_i is chosen to ensure that $\Gamma_1(x) \geq \eta_i x$ as shown in Figure 2. Integrating $y = \Gamma_1(x)$ provides:

$$\begin{aligned} \sum_{i=1}^{n}\int_0^{\Delta q_i}\Gamma_1(x)dx &\geq \sum_{i=1}^{n}\int_0^{\Delta q_i}\eta_i x dx = \sum_{i=1}^{n}0.5\eta_i(\Delta q_i)^2 \\ &= 0.5\Delta\boldsymbol{q}^T\boldsymbol{\eta}\Delta\boldsymbol{q} \end{aligned} \tag{8}$$

Function $y = \Gamma_2(x)$ is shown in Figure 3, when $x \in [r_j\ r_{j+1}]$ $j=1, 2, \ldots, r_0 = 0, \alpha_j(x\text{-}r_j) \leq \Gamma_2(x) \leq \beta_j(x - r_j), [0\ \Delta q_i] = [0\ r_2] \cup [r_2\ r_3] \cup [r_3 r_4] \cup [r_4 r_5] \ldots [r_j\ \Delta q_i]$. Integrating $y = \Gamma_2(x)$ gives:

$$\begin{aligned} \sum_{i=1}^{n}\int_0^{\Delta q_i}\Gamma_2(x)dx &= \sum_{i=1}^{n}\left(\int_0^{r_2}\Gamma_2(x) + \int_{r_2}^{r_3}\Gamma_2(x)\right. \\ &\quad \left. + \int_{r_3}^{r_4}\Gamma_2(x) + \cdots + \int_{r_j}^{\Delta q_i}\Gamma_2(x)\right)dx \\ &\geq \sum_{i=1}^{n}\left(\int_0^{r_2}\alpha_1 x + \int_{r_2}^{r_3}\alpha_2(x - r_2)\right. \\ &\quad + \int_{r_3}^{r_4}\alpha_3(x - r_3) + \cdots \\ &\quad \left. + \int_{r_j}^{\Delta q_i}\alpha_j(x - r_j)\right)dx \\ &= \sum_{i=1}^{n}\left(0.5\alpha_1 r_2^2 + 0.5\alpha_2(r_3 - r_2)^2\right. \\ &\quad + 0.5\alpha_3(r_4 - r_3)^2 + \cdots \\ &\quad \left. + 0.5\alpha_j(\Delta q_i - r_j)^2\right) \\ &\geq \sum_{i=1}^{n}0.5\alpha_j(\Delta q_i - r_j)^2 \end{aligned} \tag{9}$$

where, r_{ii} is the corresponding x value of the minimum of y $= \Gamma_2(x)$, $\alpha_i = \min(\Gamma_2(r_{ii}))/(r_{ii} - r_i)$, $x \in [r_i \infty)$.

As shown in Figure 3, when $x \in [\Gamma_2(x)/\beta_j + r_j, \Gamma_2(x)/\beta_{j+1} + r_{j+1}]$, j = 1,2,…, $r_0 = 0$, $\alpha_j(x - r_j) \le \Gamma_2(x) \le \beta_j(x - r_j)$, yields:

$$\begin{aligned}&\boldsymbol{\Gamma}_2^T(\Delta\boldsymbol{q})\boldsymbol{M}(\boldsymbol{q})\boldsymbol{\Gamma}_2(\Delta\boldsymbol{q})\\ &\le \sum_{i=1}^{n}\Gamma_2(\Delta q_i)\lambda_{\max}\|\boldsymbol{M}(\boldsymbol{q})\|\Gamma_2(\Delta q_i)\\ &\le \sum_{i=1}^{n}(\Delta q_i - r_j)\lambda_{\max}(\beta_j)\lambda_{\max}\|\boldsymbol{M}(\boldsymbol{q})\|\lambda_{\max}(\beta_j)(\Delta q_i - r_j)\end{aligned} \tag{10}$$

As shown in Figure 3, $\Delta\dot{\boldsymbol{q}} = \dot{\boldsymbol{q}}_d - \dot{\boldsymbol{q}} = -\dot{\boldsymbol{q}}$, yields:

$$\begin{aligned}-\left(\dot{\boldsymbol{\Gamma}}_2(\Delta\boldsymbol{q})\Delta\dot{\boldsymbol{q}}\right)^{\mathrm{T}}\boldsymbol{M}(\boldsymbol{q})\dot{\boldsymbol{q}} &= \dot{\boldsymbol{\Gamma}}_2^T(\Delta\boldsymbol{q})\dot{\boldsymbol{q}}^{\mathrm{T}}\boldsymbol{M}(\boldsymbol{q})\dot{\boldsymbol{q}}\\ &\le \dot{\boldsymbol{q}}^T\lambda_{\max}(\gamma_j)\lambda_{\max}\|\boldsymbol{M}(\boldsymbol{q})\|\dot{\boldsymbol{q}}\end{aligned} \tag{11}$$

where $\lambda_{\max}(\gamma_j)$ is the maximum derivative of y $= \Gamma_2(x)$.

As $\boldsymbol{\Gamma}_2(\Delta\boldsymbol{q}) \le \boldsymbol{M}_1$, $\|\boldsymbol{\Gamma}_2(\Delta\boldsymbol{q})\| \le \sqrt{n}M_1$ can be deduced, yields:

$$-\boldsymbol{\Gamma}_2^T(\Delta\boldsymbol{q})\boldsymbol{C}(\boldsymbol{q},\dot{\boldsymbol{q}})\dot{\boldsymbol{q}} \le \sqrt{n}M_1C_M\|\dot{\boldsymbol{q}}\|^2 \tag{12}$$

where M_1 is the maximum of the saturated function y $= \Gamma_2(x)$. C_M is a positive constant.

III. STABILITY ANALYSIS OF NONLINEAR PID CONTROL

A. STABILITY ANALYSIS OF LINEAR D + NONLINEAR PI

The control law can be written as

$$\boldsymbol{\tau} = \boldsymbol{K}_P\boldsymbol{\Gamma}_1(\Delta\boldsymbol{q}) + \boldsymbol{K}_D\Delta\dot{\boldsymbol{q}} + \boldsymbol{K}_I\int_0^t\boldsymbol{\Gamma}_2(\Delta\boldsymbol{q}(\sigma))d\sigma \tag{13}$$

where $\boldsymbol{K}_P$, $\boldsymbol{K}_D$, and $\boldsymbol{K}_I$ are suitable positive definite diagonal n×n matrices, $\boldsymbol{q} = \boldsymbol{q}_d - \boldsymbol{q}$ is the position errors vector.

The following vector is introduced as follows:

$$z(t) = \int_0^t\boldsymbol{\Gamma}_2(\Delta\boldsymbol{q}(\sigma))d\sigma - \boldsymbol{K}_I^{-1}\boldsymbol{g}(\boldsymbol{q}_d) \tag{14}$$

where $\boldsymbol{g}(\boldsymbol{q}_d)$ is the desired gravity torque vector.

By substituting (13) and (14) into the robot dynamics (7), we obtain

$$\begin{aligned}&\boldsymbol{M}(\boldsymbol{q})\ddot{\boldsymbol{q}} + \boldsymbol{C}(\boldsymbol{q},\dot{\boldsymbol{q}})\dot{\boldsymbol{q}} + \boldsymbol{D}\dot{\boldsymbol{q}} + \boldsymbol{g}(\boldsymbol{q}) - \boldsymbol{g}(\boldsymbol{q}_d)\\ &\qquad -\boldsymbol{K}_P\boldsymbol{\Gamma}_1(\Delta\boldsymbol{q}) - \boldsymbol{K}_Iz - \boldsymbol{K}_D\Delta\dot{\boldsymbol{q}} = 0\end{aligned} \tag{15}$$

The state-space formulation of the equation (15) can be expressed as

$$\begin{aligned}\frac{d}{dt}\begin{bmatrix}\Delta\boldsymbol{q}\\ \dot{\boldsymbol{q}}\\ z\end{bmatrix} &= \begin{bmatrix}-\dot{\boldsymbol{q}}\\ \boldsymbol{M}(\boldsymbol{q})^{-1}\begin{pmatrix}\boldsymbol{g}(\boldsymbol{q}_d) - \boldsymbol{g}(\boldsymbol{q}) + \boldsymbol{K}_P\boldsymbol{\Gamma}_1(\Delta\boldsymbol{q})\\ +\boldsymbol{K}_Iz - \boldsymbol{K}_D\dot{\boldsymbol{q}} - \boldsymbol{C}(\boldsymbol{q},\dot{\boldsymbol{q}})\dot{\boldsymbol{q}} - \boldsymbol{D}\dot{\boldsymbol{q}}\end{pmatrix}\\ \boldsymbol{\Gamma}_2(\Delta\boldsymbol{q})\end{bmatrix}\\ &= \begin{bmatrix}\dot{\boldsymbol{q}}\\ \ddot{\boldsymbol{q}}\\ \boldsymbol{\Gamma}_2(\Delta\boldsymbol{q})\end{bmatrix}\end{aligned} \tag{16}$$

The equation (16) is an autonomous nonlinear differential equation. The vector $\left[\Delta\boldsymbol{q}^T\dot{\boldsymbol{q}}^Tz^T\right]$ is the equilibrium point of equation (16) if

$$\frac{d}{dt}\begin{bmatrix}\Delta\boldsymbol{q}\\ \dot{\boldsymbol{q}}\\ z\end{bmatrix} = 0 \tag{17}$$

Based on (16) and (17), $\dot{\boldsymbol{q}} = 0$, $\boldsymbol{\Gamma}_2(\Delta\boldsymbol{q}) = 0$. Base on the definition of $\boldsymbol{\Gamma}_2(x)$, $\boldsymbol{q}$=$\boldsymbol{0}$ can be obtained. Based on the equations $\dot{\boldsymbol{q}} = 0$, $\Delta\boldsymbol{q} = 0$, and Equation (18) can be obtained as follow:

$$\begin{aligned}&\boldsymbol{g}(\boldsymbol{q}_d) - \boldsymbol{g}(\boldsymbol{q}) + \boldsymbol{K}_P\boldsymbol{\Gamma}_1(\Delta\mathbf{q}) + \boldsymbol{K}_Iz\\ &\qquad -\boldsymbol{K}_D\dot{q} - \boldsymbol{C}(\boldsymbol{q},\dot{\boldsymbol{q}})\dot{\boldsymbol{q}} - \boldsymbol{D}\dot{\boldsymbol{q}} = 0\end{aligned} \tag{18}$$

$z = \boldsymbol{0}$ can be obtained. The equilibrium point is $\left[\Delta\boldsymbol{q}^T\dot{\boldsymbol{q}}^Tz^T\right]^{\mathrm{T}} = 0$.

Theorem For the nonlinear robot system defined by (7), the state feedback NPDNI controller as defined (13) is adopted, there exist enough small positive constants a, and the $\boldsymbol{K}_P$, $\boldsymbol{K}_D$, and $\boldsymbol{K}_I$ are appropriately selected and the inequalities (19)~(22) are satisfied, the closed-loop system is globally asymptotically stable, i. e. $\lim_{t\to\infty}\Delta\boldsymbol{q} = 0$.

$$\begin{aligned}&\lambda_{\min}(\alpha_j)(\boldsymbol{K}_D + \boldsymbol{D})\\ &\quad \ge 2\lambda_{\max}(\beta_j)\lambda_{\max}\|\boldsymbol{M}(\boldsymbol{q})\|\lambda_{\max}(\beta_j)\boldsymbol{I}\end{aligned} \tag{19}$$

$$\begin{aligned}&\boldsymbol{U}(\boldsymbol{q}) - \boldsymbol{U}(\boldsymbol{q}_d) + \Delta\boldsymbol{q}^T\boldsymbol{g}(\boldsymbol{q}_d) + \frac{1}{2}\Delta\boldsymbol{q}^{\mathrm{T}}(\boldsymbol{K}_P\boldsymbol{\eta} - \boldsymbol{K}_I)\Delta\boldsymbol{q}\\ &\quad \ge a\|\Delta\boldsymbol{q}\|^2\end{aligned} \tag{20}$$

$$\begin{aligned}&\boldsymbol{\Gamma}_2^T(\Delta\boldsymbol{q})(\boldsymbol{g}(\boldsymbol{q}_d) - \boldsymbol{g}(\boldsymbol{q}) + \boldsymbol{K}_p\boldsymbol{\Gamma}_1(\Delta\boldsymbol{q}) - \boldsymbol{K}_I\Delta\boldsymbol{q})\\ &\quad \ge a\|\boldsymbol{\Gamma}_2(\Delta\boldsymbol{q})\|^2\end{aligned} \tag{21}$$

$$\boldsymbol{K}_D + \boldsymbol{D} \ge \lambda_{\max}(\gamma_j)\lambda_{\max}\|\boldsymbol{M}(\boldsymbol{q})\|\boldsymbol{I} + \sqrt{n}M_1C_M\boldsymbol{I} \tag{22}$$

Proof: The Lyapunov function candidate is proposed as follows:

$$\begin{aligned}\boldsymbol{V} = &\frac{1}{2}\dot{\boldsymbol{q}}^{\mathrm{T}}\boldsymbol{M}(\boldsymbol{q})\dot{\boldsymbol{q}} - \boldsymbol{\Gamma}_2^{\mathrm{T}}(\Delta\boldsymbol{q})\boldsymbol{M}(\boldsymbol{q})\dot{\boldsymbol{q}} + \boldsymbol{U}(\boldsymbol{q}) - \boldsymbol{U}(\boldsymbol{q}_d)\\ &+ \Delta\boldsymbol{q}^T\boldsymbol{g}(\boldsymbol{q}_d) - \frac{1}{2}\Delta\boldsymbol{q}^{\mathrm{T}}\boldsymbol{K}_I\Delta\boldsymbol{q} + \sum_{i=1}^{n}\int_0^{\Delta q_i}\Gamma_1(x)K_{Pi}dx_i\\ &+ \sum_{i=1}^{n}\int_0^{\Delta q_i}\Gamma_2(x)(K_{Di} + D_i)dx_i\\ &+ \frac{1}{2}(z + \Delta\boldsymbol{q})^T\boldsymbol{K}_I(z + \Delta\boldsymbol{q})\end{aligned} \tag{23}$$

where K_{Pi}, K_{Di} and D_i are the ith diagonal element of $\boldsymbol{K}_P$, $\boldsymbol{K}_D$ and $\boldsymbol{D}$.

Based on (9), the following inequalities equation can be obtained as follows:

$$\begin{aligned}&\sum_{i=1}^{n}\int_0^{\Delta q_i}\Gamma_2(x)(K_{Di} + D_i)\mathrm{d}x\\ &\qquad \ge \sum_{i=1}^{n}0.5\alpha_j(\Delta q_i - r_j)^2(K_{Di} + D_i)\end{aligned} \tag{24}$$

where α_j satisfies $0 < \alpha_j \le \Gamma_2(\Delta q_j)/\Delta q_j$.

Based on (8), the following inequalities equation can be obtained as follows:

$$\sum_{i=1}^{n}\int_0^{\Delta q_i}\Gamma_1(x)K_{\mathrm{P}i}dx_i-\frac{1}{2}\Delta\boldsymbol{q}^{\mathrm{T}}\boldsymbol{K}_{\mathrm{I}}\Delta\boldsymbol{q}\geq\sum_{i=1}^{n}\int_0^{\Delta q_i}K_{\mathrm{P}i}\eta_i x dx$$
$$-\frac{1}{2}\Delta\boldsymbol{q}^{\mathrm{T}}\boldsymbol{K}_{\mathrm{I}}\Delta\boldsymbol{q}=\frac{1}{2}\sum_{i=1}^{n}\Delta q_i K_{\mathrm{P}i}\eta_i\Delta q_i-\frac{1}{2}\Delta\boldsymbol{q}^{\mathrm{T}}\boldsymbol{K}_{\mathrm{I}}\Delta\boldsymbol{q}=\frac{1}{2}\Delta\boldsymbol{q}^{\mathrm{T}}\left(\boldsymbol{K}_{\mathrm{P}}\boldsymbol{\eta}-\boldsymbol{K}_{\mathrm{I}}\right)\Delta\boldsymbol{q}\tag{25}$$

where η satisfies $0<\eta_i\leq\Gamma_1(\Delta q_i)/\Delta q_i$.

Based on (10) and (24), the following inequalities can be obtained as follows:

$$\begin{aligned}&\frac{1}{4}\dot{\boldsymbol{q}}^T\boldsymbol{M}(\boldsymbol{q})\dot{\boldsymbol{q}}-\boldsymbol{\Gamma}_2^T(\Delta\boldsymbol{q})\boldsymbol{M}(\boldsymbol{q})\dot{\boldsymbol{q}}\\&\quad+\sum_{i=1}^{n}\int_0^{\Delta q_i}\Gamma_2(x)(K_{\mathrm{D}i}+D_i)\mathrm{d}x\\&=\sum_{i=1}^{n}\int_0^{\Delta q_i}\Gamma_2(x)(K_{\mathrm{D}i}+D_i)\mathrm{d}x-\boldsymbol{\Gamma}_2^T(\Delta\boldsymbol{q})\boldsymbol{M}(\boldsymbol{q})\boldsymbol{\Gamma}_2(\Delta\boldsymbol{q})\\&\quad+\frac{1}{4}(\dot{\boldsymbol{q}}-2\boldsymbol{\Gamma}_2(\Delta\boldsymbol{q}))^T\boldsymbol{M}(q)(\dot{\boldsymbol{q}}-2\boldsymbol{\Gamma}_2(\Delta\boldsymbol{q}))\\&\geq\sum_{i=1}^{n}(\Delta q_i-r_j)\begin{pmatrix}0.5\lambda_{\min}(\alpha_j)(K_{\mathrm{D}i}+D_i)\\-\lambda_{\max}(\beta_j)\lambda_{\max}\|\boldsymbol{M}(q)\|\lambda_{\max}(\beta_j)\end{pmatrix}\\&\quad\times(\Delta q_i-r_j)\end{aligned}\tag{26}$$

By substituting inequalities (25) and (26) into (23), when $\left[\Delta\boldsymbol{q}^T\dot{\boldsymbol{q}}^Tz^T\right]^{\mathrm{T}}\neq0$, we get

$$\begin{aligned}\boldsymbol{V}=&\frac{1}{4}\dot{\boldsymbol{q}}^T\boldsymbol{M}(\boldsymbol{q})\dot{\boldsymbol{q}}+\Big(\boldsymbol{U}(\boldsymbol{q})-\boldsymbol{U}(\boldsymbol{q}_{\mathrm{d}})+\Delta\boldsymbol{q}^T\boldsymbol{g}(\boldsymbol{q}_{\mathrm{d}})\\&+\sum_{i=1}^{n}\int_0^{\Delta q_i}\Gamma_1(x)K_{\mathrm{P}i}dx_i-\frac{1}{2}\Delta\boldsymbol{q}^T\boldsymbol{K}_{\mathrm{I}}\Delta\boldsymbol{q}\Big)\\&+\Big(\frac{1}{4}\dot{\boldsymbol{q}}^T\boldsymbol{M}(\boldsymbol{q})\dot{\boldsymbol{q}}+\boldsymbol{\Gamma}_2^T(\Delta q)\boldsymbol{M}(\boldsymbol{q})\dot{\boldsymbol{q}}\\&\times\sum_{i=1}^{n}\int_0^{\Delta q_i}\Gamma_2(x)(K_{Di}+D_i)dx\Big)\\&+\frac{1}{2}(z+\Delta\boldsymbol{q})^T\boldsymbol{K}_{\mathrm{I}}(z+\Delta\boldsymbol{q})\geq a\|\boldsymbol{\Gamma}_2(\Delta\boldsymbol{q})\|^2\\&+\frac{1}{2}(z+\Delta\boldsymbol{q})^T\boldsymbol{K}_{\mathrm{I}}(z+\Delta\boldsymbol{q})\\&+\sum_{i=1}^{n}(\Delta q_i-r_j)\left(0.5\lambda_{\min}(\alpha_j)(K_{Di}+D_i)\right.\\&\left.-\left(\lambda_{\max}(\beta_j)\lambda_{\max}\|\boldsymbol{M}(q)\|\lambda_{\max}(\beta_j)\right)(\Delta q_i-r_j)\right)>0\end{aligned}\tag{27}$$

Therefore, the Lyapunov function defined by (23) is the positive definite, when $\left[\Delta\boldsymbol{q}^T\dot{\boldsymbol{q}}^Tz^T\right]\to\infty,\ \boldsymbol{V}\to\infty$.

The time derivative of (23) along the closed-loop system (15) results in

$$\begin{aligned}\dot{\boldsymbol{V}}=&\frac{1}{2}\dot{\boldsymbol{q}}^T\dot{\boldsymbol{M}}(\boldsymbol{q})\dot{\boldsymbol{q}}+\dot{\boldsymbol{q}}^T\boldsymbol{M}(\boldsymbol{q})\ddot{\boldsymbol{q}}-\left(\dot{\boldsymbol{\Gamma}}_2(\Delta\boldsymbol{q})\Delta\dot{\boldsymbol{q}}\right)^T\boldsymbol{M}(\boldsymbol{q})\dot{\boldsymbol{q}}\\&+\dot{\boldsymbol{q}}^T\boldsymbol{g}(\boldsymbol{q})-\boldsymbol{\Gamma}_2^T(\Delta\boldsymbol{q})\boldsymbol{M}(\boldsymbol{q})\ddot{\boldsymbol{q}}+\Delta\dot{\boldsymbol{q}}^T\boldsymbol{g}(\boldsymbol{q}_{\mathrm{d}})\\&+\Delta\dot{\boldsymbol{q}}^T\boldsymbol{K}_{\mathrm{P}}\boldsymbol{\Gamma}_1(\Delta\boldsymbol{q})-\boldsymbol{\Gamma}_2^T(\Delta\boldsymbol{q})\dot{\boldsymbol{M}}(\boldsymbol{q})\dot{\boldsymbol{q}}\\&+\Delta\dot{\boldsymbol{q}}^T(\boldsymbol{K}_{\mathrm{D}}+\boldsymbol{D})\boldsymbol{\Gamma}_2(\Delta\boldsymbol{q})-\Delta\dot{\boldsymbol{q}}^T\boldsymbol{K}_{\mathrm{I}}\Delta\boldsymbol{q}\\&+(\dot{z}+\Delta\dot{\boldsymbol{q}})^T\boldsymbol{K}_{\mathrm{I}}(z+\Delta\boldsymbol{q})\end{aligned}\tag{28}$$

By substituting (14) and (15) into (28), we obtain

$$\begin{aligned}\dot{\boldsymbol{V}}=&-\dot{\boldsymbol{q}}^{\mathrm{T}}(\boldsymbol{D}+\boldsymbol{K}_{\mathrm{D}})\dot{\boldsymbol{q}}-\left(\dot{\boldsymbol{\Gamma}}_2(\Delta\boldsymbol{q})\Delta\dot{\boldsymbol{q}}\right)^T\boldsymbol{M}(\boldsymbol{q})\dot{\boldsymbol{q}}\\&-\boldsymbol{\Gamma}_2^T(\Delta\boldsymbol{q})\boldsymbol{C}(\boldsymbol{q},\dot{\boldsymbol{q}})\dot{\boldsymbol{q}}-\boldsymbol{\Gamma}_2^T(\Delta\boldsymbol{q})\left(\boldsymbol{g}(\boldsymbol{q}_{\mathrm{d}})-\boldsymbol{g}(\boldsymbol{q})\right.\\&\left.+\boldsymbol{K}_P\boldsymbol{\Gamma}_1(\Delta\boldsymbol{q})-\boldsymbol{K}_{\mathrm{I}}\Delta\boldsymbol{q}\right)\end{aligned}\tag{29}$$

By substituting (11) and (12) into (29), we obtain

$$\begin{aligned}\dot{\boldsymbol{V}}\leq&-\dot{\boldsymbol{q}}^T\left[\boldsymbol{K}_{\mathrm{D}}+\boldsymbol{D}-\lambda_{\max}(\gamma_{\mathrm{j}})\lambda_{\max}\|\boldsymbol{M}(\boldsymbol{q})\|\boldsymbol{I}\right.\\&\left.-\sqrt{n}\mathrm{M}_1\mathrm{C}_{\mathrm{M}}\boldsymbol{I}\right]\dot{\boldsymbol{q}}-a\|\boldsymbol{\Gamma}_2(\Delta\boldsymbol{q})\|^2\end{aligned}\tag{30}$$

Based on inequality (21) and (22), a >0, the conclusion that $\dot{\boldsymbol{V}}\leq0$ can be obtained. In fact $\dot{\boldsymbol{V}}=0$ means $\Delta\boldsymbol{q}=0$ and $\dot{\boldsymbol{q}}=0$. Based LaSalle's invariance principle, it is easy to know that $(\Delta\boldsymbol{q}=0,\ \dot{\boldsymbol{q}}=0)$ is the global asymptotic equilibrium position.

B. STABILITY ANALYSIS OF LINEAR PD + NONLINEAR PI

The control law can be written as

$$\begin{aligned}\boldsymbol{\tau}=&\boldsymbol{K}_{\mathrm{P}}\boldsymbol{\Gamma}_1(\Delta\boldsymbol{q})+\boldsymbol{K}_{\mathrm{D}}\Delta\dot{\boldsymbol{q}}+\int_0^t[\boldsymbol{K}_{\mathrm{IP}}\boldsymbol{\Gamma}_2(\Delta\boldsymbol{q}(\sigma))\\&+\boldsymbol{K}_{\mathrm{ID}}\Delta\dot{\boldsymbol{q}}(\sigma)]\mathrm{d}\sigma\end{aligned}\tag{31}$$

where $\boldsymbol{K}_{\mathrm{P}}$, $\boldsymbol{K}_{\mathrm{D}}$, $\boldsymbol{K}_{\mathrm{IP}}$, and $\boldsymbol{K}_{\mathrm{ID}}$ are suitable positive definite diagonal n×n matrices.

The following vector is introduced as follows:

$$z(t)=\Delta\boldsymbol{q}+\int_0^t\boldsymbol{\Gamma}_2(\Delta\boldsymbol{q}(\boldsymbol{\sigma}))\,\mathrm{d}\sigma-\boldsymbol{K}_{\mathrm{IP}}^{-1}\boldsymbol{g}(\boldsymbol{q}_{\mathrm{d}})\tag{32}$$

By substituting (31) and (32) into the robot dynamics (7), we obtain

$$\begin{aligned}&\boldsymbol{M}(\boldsymbol{q})\ddot{\boldsymbol{q}}+\boldsymbol{C}(\boldsymbol{q},\dot{\boldsymbol{q}})\dot{\boldsymbol{q}}+\boldsymbol{D}\dot{\boldsymbol{q}}+\boldsymbol{g}(\boldsymbol{q})-\boldsymbol{g}(\boldsymbol{q}_{\mathrm{d}})-\boldsymbol{K}_P\boldsymbol{\Gamma}_1(\Delta\boldsymbol{q})\\&\quad-(\boldsymbol{K}_{ID}-\boldsymbol{K}_{IP})\Delta\boldsymbol{q}-\boldsymbol{K}_{IP}z-\boldsymbol{K}_D\Delta\dot{\boldsymbol{q}}=0\end{aligned}\tag{33}$$

The state-space formulation of the equation (33) can be expressed as

$$\begin{aligned}&\frac{d}{dt}\begin{bmatrix}\Delta\boldsymbol{q}\\\dot{\boldsymbol{q}}\\z\end{bmatrix}\\&=\begin{bmatrix}-\dot{\boldsymbol{q}}\\\boldsymbol{M}(\boldsymbol{q})^{-1}\begin{pmatrix}\boldsymbol{g}(\boldsymbol{q}_d)-\boldsymbol{g}(\boldsymbol{q})+\boldsymbol{K}_{\mathrm{P}}\boldsymbol{\Gamma}_1(\Delta\boldsymbol{q})+\boldsymbol{K}_{\mathrm{I}}z-\boldsymbol{K}_{\mathrm{D}}\dot{\boldsymbol{q}}\\+(\boldsymbol{K}_{\mathrm{ID}}-\boldsymbol{K}_{\mathrm{IP}})\Delta\boldsymbol{q}-\boldsymbol{C}(\boldsymbol{q},\dot{\boldsymbol{q}})\dot{\boldsymbol{q}}-\boldsymbol{D}\dot{\boldsymbol{q}}\end{pmatrix}\\-\dot{\boldsymbol{q}}+\boldsymbol{\Gamma}_2(\Delta\boldsymbol{q})\end{bmatrix}\end{aligned}\tag{34}$$

The equation (34) is an autonomous nonlinear differential equation. The vector $\left[\Delta \boldsymbol{q}^T \dot{\boldsymbol{q}}^T \boldsymbol{z}^T\right]$ is the equilibrium point of equation (34) if

$$\frac{d}{dt}\begin{bmatrix}\Delta \boldsymbol{q}\\ \dot{\boldsymbol{q}}\\ \boldsymbol{z}\end{bmatrix} = 0 \tag{35}$$

Based on (34) and (35), $\dot{\boldsymbol{q}} = 0,\ \Gamma_2(\Delta \boldsymbol{q}) - \dot{\boldsymbol{q}} = 0$. Base on the definition of Γ_2(x), $\boldsymbol{q} = \boldsymbol{0}$ can be obtained. Based on the equations $\dot{\boldsymbol{q}} = 0,\ \Delta \boldsymbol{q} = 0$, and Equation (36) can be obtained as follow:

$$\begin{aligned}&\boldsymbol{g}(\boldsymbol{q_d}) - \boldsymbol{g}(\boldsymbol{q}) + \boldsymbol{K}_P \boldsymbol{\Gamma}_1(\Delta \boldsymbol{q}) + \boldsymbol{K}_I \boldsymbol{z} - \boldsymbol{K}_D \dot{\boldsymbol{q}}\\ &\quad + (\boldsymbol{K}_{ID} - \boldsymbol{K}_{IP})\Delta \boldsymbol{q} - \boldsymbol{C}(\boldsymbol{q}, \dot{\boldsymbol{q}})\dot{\boldsymbol{q}} - \boldsymbol{D}\dot{\boldsymbol{q}} = 0\end{aligned} \tag{36}$$

$\boldsymbol{z} = 0$ can be obtained. The equilibrium point is $\left[\Delta \boldsymbol{q}^T \dot{\boldsymbol{q}}^T \boldsymbol{z}^T\right]^{\mathrm{T}} = 0$.

Theorem For the nonlinear robot system defined by (7), the state feedback NPPDNI controller as defined (31) is adopted, there exist enough small positive constants a, and the $\boldsymbol{K}_{\mathrm{P}}$, $\boldsymbol{K}_{\mathrm{D}}$, $\boldsymbol{K}_{\mathrm{IP}}$, and $\boldsymbol{K}_{\mathrm{ID}}$ are appropriately selected and the inequalities (37)∼(40) are satisfied, the closed-loop system is globally asymptotically stable, i. e. $\lim_{t\to\infty} \Delta \boldsymbol{q} = 0$.

$$\begin{aligned}&\lambda_{\min}(\alpha_j)(\boldsymbol{K}_{\mathrm{D}} + \boldsymbol{D})\\ &\quad \geq 2\lambda_{\max}(\beta_j)\lambda_{\max}\|\boldsymbol{M}(\boldsymbol{q})\|\lambda_{\max}(\beta_j)\boldsymbol{I}\end{aligned} \tag{37}$$

$$\begin{aligned}&\boldsymbol{U}(\boldsymbol{q}) - \boldsymbol{U}(\boldsymbol{q}_{\mathrm{d}}) + \frac{1}{2}\Delta \boldsymbol{q}^T(\boldsymbol{K}_{\mathrm{P}}\boldsymbol{\eta} + \boldsymbol{K}_{\mathrm{ID}} - \boldsymbol{K}_{\mathrm{IP}})\Delta \boldsymbol{q}\\ &\quad + \Delta \boldsymbol{q}^{\boldsymbol{T}}\boldsymbol{g}(\boldsymbol{q}_{\mathrm{d}}) \geq a\|\Delta \boldsymbol{q}\|^2\end{aligned} \tag{38}$$

$$\begin{aligned}&\boldsymbol{\Gamma}_2(\Delta \boldsymbol{q})^T\left(\boldsymbol{g}(\boldsymbol{q}_{\mathrm{d}}) - \boldsymbol{g}(\boldsymbol{q}) + \boldsymbol{K}_{\mathrm{P}}\boldsymbol{\Gamma}_1(\Delta \boldsymbol{q})\right)\\ &\quad + \boldsymbol{\Gamma}_2(\Delta \boldsymbol{q})^T(\boldsymbol{K}_{\mathrm{ID}} - \boldsymbol{K}_{\mathrm{IP}})\Delta \boldsymbol{q} \geq a\|\boldsymbol{\Gamma}_2(\Delta \boldsymbol{q})\|^2\end{aligned} \tag{39}$$

$$\begin{aligned}&\boldsymbol{K}_{\mathrm{D}} + \boldsymbol{D}\\ &\quad \geq \lambda_{\max}(\gamma_j)\lambda_{\max}\|\boldsymbol{M}(\boldsymbol{q})\|\boldsymbol{I} + \sqrt{n}\mathrm{M}_1\mathrm{C}_{\mathrm{M}}\boldsymbol{I}\end{aligned} \tag{40}$$

Proof: The Lyapunov function candidate is proposed as follows:

$$\begin{aligned}\boldsymbol{V} =\ &\frac{1}{2}\dot{\boldsymbol{q}}^{\mathrm{T}}\boldsymbol{M}(\boldsymbol{q})\dot{\boldsymbol{q}} - \boldsymbol{\Gamma}_2(\Delta \boldsymbol{q})^{\mathrm{T}}\boldsymbol{M}(\boldsymbol{q})\dot{\boldsymbol{q}} + \mathrm{U}(\boldsymbol{q}) - \boldsymbol{U}(\boldsymbol{q}_{\mathrm{d}})\\ &+ \Delta \boldsymbol{q}^T\boldsymbol{g}(\boldsymbol{q}_{\mathrm{d}}) + \frac{1}{2}\boldsymbol{z}^T\boldsymbol{K}_{\mathrm{IP}}\boldsymbol{z} + \frac{1}{2}\Delta \boldsymbol{q}^T(\boldsymbol{K}_{\mathrm{ID}} - \boldsymbol{K}_{\mathrm{IP}})\Delta \boldsymbol{q}\\ &+ \sum_{i=1}^{n}\int_0^{\Delta q_i}\Gamma_1(x)K_{\mathrm{P}i}dx\\ &+ \sum_{i=1}^{n}\int_0^{\Delta q_i}\Gamma_2(x)(K_{\mathrm{D}i} + D_i)dx\end{aligned} \tag{41}$$

where $K_{\mathrm{P}i}$, $K_{\mathrm{D}i}$ and D_i are the ith diagonal element of $\boldsymbol{K}_{\mathrm{P}}$, $\boldsymbol{K}_{\mathrm{D}}$ and $\boldsymbol{D}$.

Based on (9), the following inequalities equation can be obtained as follows:

$$\begin{aligned}&\sum_{i=1}^{n}\int_0^{\Delta q_i}\Gamma_2(x)(K_{\mathrm{D}i} + D_i)\mathrm{d}x\\ &\qquad \geq \sum_{i=1}^{n}0.5\alpha_j(\Delta q_i - r_j)^2(K_{\mathrm{D}i} + D_i)\end{aligned} \tag{42}$$

where α_{i} satisfies $0 < \alpha_j \leq \Gamma_1(\Delta q_j)/\Delta q_j$.

Based on (10) and (42), the following inequalities can be obtained as follows:

$$\begin{aligned}&\frac{1}{4}\dot{\boldsymbol{q}}^T\boldsymbol{M}(\boldsymbol{q})\dot{\boldsymbol{q}} - \boldsymbol{\Gamma}_2^T(\Delta \boldsymbol{q})\boldsymbol{M}(\boldsymbol{q})\dot{\boldsymbol{q}}\\ &\quad + \sum_{i=1}^{n}\int_0^{\Delta q_i}\Gamma_2(x)(K_{\mathrm{D}i} + D_i)\mathrm{d}x\\ &= \sum_{i=1}^{n}\int_0^{\Delta q_i}\Gamma_2(x)(K_{\mathrm{D}i} + D_i)\mathrm{d}x - \boldsymbol{\Gamma}_2^T(\Delta \boldsymbol{q})\boldsymbol{M}(\boldsymbol{q})\boldsymbol{\Gamma}_2(\Delta \boldsymbol{q})\\ &\quad + \frac{1}{4}(\dot{\boldsymbol{q}} - 2\boldsymbol{\Gamma}_2(\Delta \boldsymbol{q}))^T\boldsymbol{M}(q)\left(\dot{\boldsymbol{q}} - 2\boldsymbol{\Gamma}_2^T(\Delta \boldsymbol{q})\right)\\ &\geq \sum_{i=1}^{n}(\Delta q_i - r_j)\left(0.5\lambda_{\min}(\alpha_j)(K_{\mathrm{D}i} + D_i)\right)(\Delta q_i - r_j)\\ &\quad - \sum_{i=1}^{n}(\Delta q_i - r_j)\left(\lambda_{\max}(\beta_j)\lambda_{\max}\|\boldsymbol{M}(q)\|\lambda_{\max}(\beta_j)\right)\\ &\quad \times (\Delta q_i - r_j)\end{aligned} \tag{43}$$

By substituting inequalities (42) and (43) into (41), when $\left[\Delta \boldsymbol{q}^T \dot{\boldsymbol{q}}^T \boldsymbol{z}^T\right]^{\mathrm{T}} \neq 0$, we get

$$\begin{aligned}\boldsymbol{V} \geq\ &-\sum_{i=1}^{n}(\Delta q_i - r_j)\left(\lambda_{\max}(\beta_j)\lambda_{\max}\|\boldsymbol{M}(q)\|\lambda_{\max}(\beta_j)\right)\\ &\times (\Delta q_i - r_j)) + \frac{1}{2}\boldsymbol{z}^T\boldsymbol{K}_{\mathrm{IP}}\boldsymbol{z} + \big(\boldsymbol{U}(\boldsymbol{q}) - \boldsymbol{U}(\boldsymbol{q}_{\mathrm{d}})\\ &+ \Delta \boldsymbol{q}^T\boldsymbol{g}(\boldsymbol{q}_{\mathrm{d}}) + \frac{1}{2}\Delta \boldsymbol{q}^T(\boldsymbol{K}_{\mathrm{P}}\boldsymbol{\eta} + \boldsymbol{K}_{ID} - \boldsymbol{K}_{IP})\Delta \boldsymbol{q}\big)\\ &+ \sum_{i=1}^{n}(\Delta q_i - r_j)(0.5\lambda_{\min}(\alpha_i)(K_{\mathrm{D}i} + D_i))(\Delta q_i - r_j)\\ &+ \frac{1}{4}\dot{\boldsymbol{q}}^T\boldsymbol{M}(\boldsymbol{q})\dot{\boldsymbol{q}}\\ \geq\ &\sum_{i=1}^{n}(\Delta q_i - r_j)\left(0.5\lambda_{\min}(\alpha_j)(K_{\mathrm{D}i} + D_i)\ (\Delta q_i - r_j)\right)\\ &- \sum_{i=1}^{n}(\Delta q_i - r_j)\left(\lambda_{\max}(\beta_j)\lambda_{\max}\|\boldsymbol{M}(q)\|\lambda_{\max}(\beta_j)\right)\\ &\times (\Delta q_i - r_j)\\ &+ \frac{1}{4}\dot{\boldsymbol{q}}^T\boldsymbol{M}(\boldsymbol{q})\dot{\boldsymbol{q}} + \frac{1}{2}\boldsymbol{z}^T\boldsymbol{K}_{\mathrm{IP}}\boldsymbol{z} + a\|\boldsymbol{\Gamma}_2(\Delta \boldsymbol{q})\|^2 > 0\end{aligned} \tag{44}$$

Therefore, the Lyapunov function defined by (41) is the positive definite. When $\left[\Delta \boldsymbol{q}^T \dot{\boldsymbol{q}}^T \boldsymbol{z}^T\right] \to \infty,\ \boldsymbol{V} \to \infty$.

The time derivative of (41) along the closed-loop system (33) results in

$$\begin{aligned}\dot{\boldsymbol{V}} =\ &\frac{1}{2}\dot{\boldsymbol{q}}^{\mathrm{T}}\dot{\boldsymbol{M}}(\boldsymbol{q})\dot{\boldsymbol{q}} + \dot{\boldsymbol{q}}^{\mathrm{T}}\boldsymbol{M}(\boldsymbol{q})\ddot{\boldsymbol{q}} - \left(\dot{\boldsymbol{\Gamma}}_2(\Delta \boldsymbol{q})\Delta \dot{\boldsymbol{q}}\right)^T\boldsymbol{M}(\boldsymbol{q})\dot{\boldsymbol{q}}\\ &- \boldsymbol{\Gamma}_2^{\mathrm{T}}(\Delta \boldsymbol{q})\dot{\boldsymbol{M}}(\boldsymbol{q})\dot{\boldsymbol{q}} - \boldsymbol{\Gamma}^{\mathrm{T}}(\Delta \boldsymbol{q})\boldsymbol{M}(\boldsymbol{q})\ddot{\boldsymbol{q}} + \dot{\boldsymbol{q}}^T\boldsymbol{g}(\boldsymbol{q})\\ &- \Delta \dot{\boldsymbol{q}}^T\boldsymbol{g}(\boldsymbol{q}_{\mathrm{d}}).\ + \dot{\boldsymbol{q}}^{\mathrm{T}}(\boldsymbol{K}_{\mathrm{ID}} - \boldsymbol{K}_{\mathrm{IP}})\Delta \boldsymbol{q} + \Delta \dot{\boldsymbol{q}}^T(\boldsymbol{K}_{\mathrm{ID}}\\ &+ \boldsymbol{D})\boldsymbol{\Gamma}_2(\Delta \boldsymbol{q}) + \dot{\boldsymbol{z}}^T\boldsymbol{K}_{\mathrm{IP}}\boldsymbol{z} + \Delta \dot{\boldsymbol{q}}^T\boldsymbol{K}_{\mathrm{IP}}\boldsymbol{\Gamma}_1(\Delta \boldsymbol{q})\end{aligned} \tag{45}$$

By substituting (32) and (33) into (45), we obtain

$$\dot{\boldsymbol{V}} = -\dot{\boldsymbol{q}}^T(\boldsymbol{D} + \boldsymbol{K}_{\mathrm{D}})\dot{\boldsymbol{q}} - \left(\dot{\boldsymbol{\Gamma}}_2(\Delta \boldsymbol{q})\Delta \dot{\boldsymbol{q}}\right)^T\boldsymbol{M}(\boldsymbol{q})\dot{\boldsymbol{q}}$$

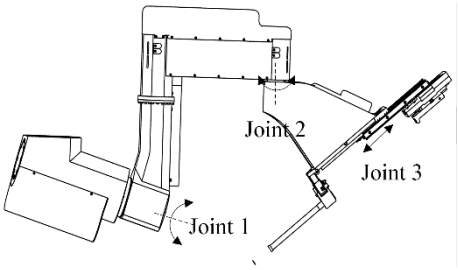

FIGURE 4. The 3D model of robot arm.

$$-\boldsymbol{\Gamma}_2^T(\Delta\boldsymbol{q})\boldsymbol{C}(\boldsymbol{q},\dot{\boldsymbol{q}})\dot{\boldsymbol{q}}-\boldsymbol{\Gamma}_2^T(\Delta\boldsymbol{q})\left(\boldsymbol{g}(\boldsymbol{q}_{\mathrm{d}})-\boldsymbol{g}(\boldsymbol{q})\right)$$
$$-\boldsymbol{\Gamma}_2^T(\Delta\boldsymbol{q})\left(\boldsymbol{K}_{\mathrm{P}}\boldsymbol{\Gamma}_1(\Delta\boldsymbol{q})+(\boldsymbol{K}_{\mathrm{ID}}-\boldsymbol{K}_{\mathrm{IP}})\Delta\boldsymbol{q}\right) \quad (46)$$

By substituting (11) and (12) into (46), we obtain

$$\dot{\boldsymbol{V}} \le -\dot{\boldsymbol{q}}^T\left[\boldsymbol{K}_{\mathrm{D}}+\boldsymbol{D}-\lambda_{\max}\left(\gamma_{\mathrm{j}}\right)\lambda_{\max}\|\boldsymbol{M}(\boldsymbol{q})\|\boldsymbol{I}\right.$$
$$\left.-\sqrt{n}\mathrm{M}_1\mathrm{C}_{\mathrm{M}}\boldsymbol{I}\right]\dot{\boldsymbol{q}}-a\|\boldsymbol{\Gamma}_2(\Delta\boldsymbol{q})\|^2 \quad (47)$$

Based on inequality(39) and (40), a>0, the conclusion that $\dot{\boldsymbol{V}} \le 0$ can be obtained. In fact $\dot{\boldsymbol{V}} = 0$ means $\Delta\boldsymbol{q} = 0$ and $\dot{\boldsymbol{q}} = 0$. Based LaSalle's invariance principle, it is easy to know that ($\Delta\boldsymbol{q} = 0$, $\dot{\boldsymbol{q}} = 0$) is the global asymptotic equilibrium position.

IV. PARAMETERS TUNING OF NONLINEAR PID

The robot arm [32] used in the simulation is shown in Figure 4, which has three degrees of freedom (DOF) with two rotational DOFs and one translational DOF. The dynamics of the robot arm can be expressed by(7).

The simulation results are employed to verify the correctness of the dynamic equation [33]. The first simulation was conducted based on (7) and an M-file was developed in Matlab software package. The second simulation was carried out using the Sim-Mechanics toolbox of Matlab. The trajectory planning used in the simulation is expressed by (48). Two simulation results are shown in Figure 5 (a) and 5 (b). The comparison between two simulation results are demonstrated in Figure 5 (c). As it can be seen, the difference between the two results is less than 0.003. Therefore, correctness of the dynamic model is verified.

$$\theta_1 = 0.4\pi\sin(0.4\pi\mathrm{t}),\ \theta_2 = -1.4\sin(0.4\pi - \mathrm{t}0.5\pi -)1.4,$$
$$d = 0.075\sin(0.4\pi\mathrm{t} - 0.5\pi) + 0.075 \quad (48)$$

PID control is the most widely applied in engineering. The PID parameter tuning is the main key issue. The multi-objective optimization based on NSGA-II is applied in this paper. The integration of the absolute value of error (IAE) between the desired and actual trajectory, and IAE between the desired and actual drive torque are chosen as the optimal objective functions as shown in (49). Taking the small mass of the third translational joint of the robot arm and simplifying calculation into consideration, the three DOFs of robot arm is simplified to two DOFs, the third joint is set the most extreme case, that is, the output torque of the second joint is the largest.

$$f_1 = \sum_{i=1}^{2}\int_0^T |\Delta q_i(t)|\mathrm{d}t \quad f_2 = \sum_{i=1}^{2}\int_0^T |\Delta u_i(t)|\mathrm{d}t \quad (49)$$

where q_{i}(t) is the error between the desired and actual trajectory, μ_{i}(t) is the error between the desired and actual drive torque.

The simulation trajectory [34] is defined by a quintic polynomial shown in (50). When t = 2s, θ_{d1} =1rad, θ_{d2} = 2rad, $\omega_{\mathrm{d1}} = \omega_{\mathrm{d2}} = 0$rad/s. When t = 4s, θ_{d1} = 0.5rad, θ_{d2} = 4rad, $\omega_{\mathrm{d1}} = \omega_{\mathrm{d2}} = 0$rad/s.

$$\theta_{d,\,j}(t) = a_0 + a_1 t + a_2 t^2 + a_3 t^3 + a_4 t^4 + a_5 t^5 \quad j = 1, 2 \quad (50)$$

Based on the definition of the general saturation function $\Gamma_2(x)$, the corresponding general saturation functions of (51) ($\Gamma_2(x)$) are expressed by (52) ($\Gamma_1(x)$).

$$y_1(x) = k_1\tanh(x)\ \ y_2(x) = \begin{cases} k_2 & when\ x \ge a_1 \\ k_2 x & others \\ -k_2 & when\ x \le -a_1 \end{cases}$$
$$y_3(x) = \begin{cases} 1 - e^{-x/\varepsilon}x \ge 0 \\ -1 + e^{x/\varepsilon}x < 0 \end{cases}$$
$$y_4(x) = \begin{cases} k_4 & when\ x \ge 0.5\pi \\ k_4\sin(x) & others \\ -k_4 & when\ x \le -0.5\pi \end{cases} \quad (51)$$
$$y_{11}(x) = k_1\tanh(x + \mathrm{sign}(x)\delta_{11}),$$
$$y_{22}(x) = \begin{cases} k_2 & when\ x \ge a_1 - \delta_{22} \\ k_2\,(x + \mathrm{sign}(x)\delta_{22}) & others \\ -k_2 & when\ x \le -a_1 + \delta_{22} \end{cases}$$
$$y_{33}(x) = \begin{cases} 1 - e^{-(x + \mathrm{sign}(x)\delta_4)/\varepsilon}x \ge 0 \\ -1 + e^{x + \mathrm{sign}(x)\delta_4/\varepsilon}x < 0 \end{cases}$$
$$y_{44}(x) = \begin{cases} k_4 & when\ x \ge 0.5\pi - \delta_{33} \\ k_4\sin(x + \mathrm{sign}(x)\delta_{33}) & others \\ -k_4 & when\ x \le -0.5\pi + \delta_{33} \end{cases} \quad (52)$$

In order to evaluate the role of the proposed general saturation function ($\boldsymbol{\Gamma_1(x)}$) in nonlinear PID control, the parameters tuning of nonlinear PID with common saturation function depicted by (51), and nonlinear PID with the proposed general saturation function defined by (52) are achieved, respectively. Firstly, the overall optimization results are compared in the tuning results, that is, the control performances (f_1 and f_2) are affected by the two different saturation functions. Second, the compromise results are chosen for comparison. The definition of the compromise solution is shown in Figure 6 [35]. The compromise solution is the point of minimum distance from the optimized solution to the utopia solution.

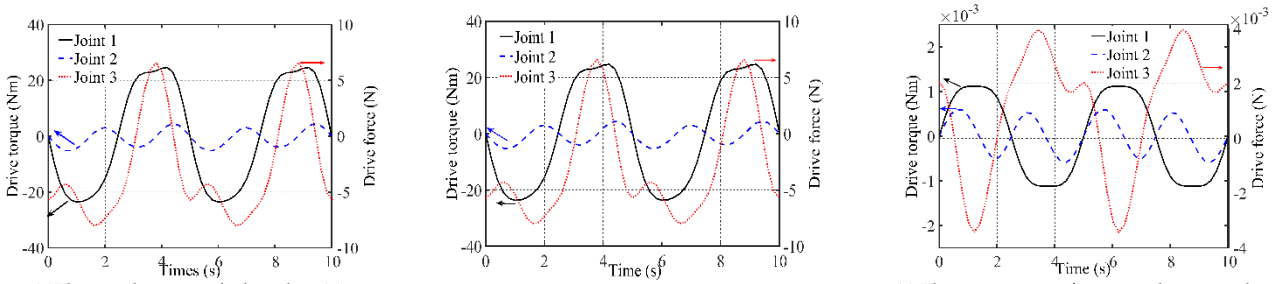

(a)The simulation results based on (7) (b) The simulation results in SimMechanics (c) The comparison of two simulation results

FIGURE 5. The simulation results of remote center motion mechanism dynamic.

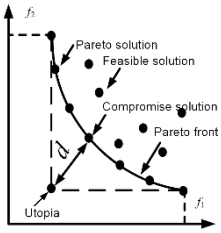

FIGURE 6. The definition of Utopia, Pareto, compromise Pareto front and feasible solution.

A. PARAMETERS TUNING OF LINEAR D + NONLINEAR PI

There are two constraints: GAS conditions are expressed by (19) $\sim$ (22) and the drive torques are less than motor rated output torques that the first and second joints are 0.18Nm and 0.05Nm.

The parameters tuning of nonlinear PID with saturation function defined by (51) and (52) are achieved by the NSGA-II. The eight groups of Pareto solutions are shown in Figure 7. By comparing (a) and (b), (c) and (d), (e) and (f), (g) and (h), it can be concluded that the trajectory tracking accuracy and the torque output accuracy of the NPDNI control law with the saturation functions defined by (52) have been improved. The Utopia solutions of NPDNI control law with saturation defined by (51) and (52) after optimization are shown in Table 1. It can be concluded that the control effect of the NPDNI control law with saturation function defined by (52) is better than that of the NPDNI control law with saturation function defined by (51). The errors between the desired output torque and actual output torque with saturation function defined by (52) are less than that with saturation function defined by(51). Compared with the trajectory tracking accuracy with saturation function defined by (51), the trajectory tracking accuracy with saturation function defined by (52) is improved by nearly an order of magnitude. In order to study the robustness of the NPDNI control law, four groups of compromise solutions shown in TABLE 2 are compared. Taking the importance of the trajectory tracking in practical application, a group (y_{11}) with high trajectory accuracy is selected to study its robustness.

B. PARAMETERS TUNING OF LINEAR PD + NONLINEAR PI

There are two constraints: GAS conditions are expressed by (37) $\sim$ (40) and the drive torques are less than motor rated output torques that the first and second joints are 0.18Nm and 0.05Nm.

The parameters tuning of nonlinear PID with saturation function defined by (51) and (52) are achieved by the NSGA-II. The eight groups of Pareto solutions are shown

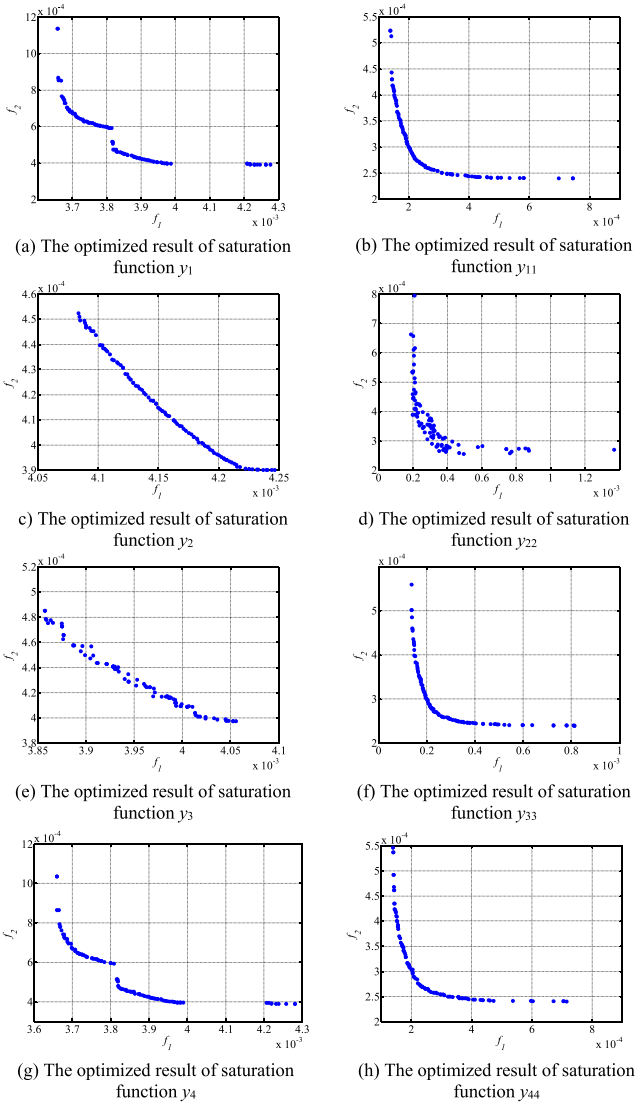

(a) The optimized result of saturation function y_1 (b) The optimized result of saturation function y_{11} c) The optimized result of saturation function y_2 d) The optimized result of saturation function y_{22} (e) The optimized result of saturation function y_3 (f) The optimized result of saturation function y_{33} (g) The optimized result of saturation function y_4 (h) The optimized result of saturation function y_{44}

FIGURE 7. The optimized result of the NPDNI control law.

TABLE 1. The Utopia points of NPDNI control law with saturation defined by (51) and (52) after optimization.

	y_1	y_{11}	y_2	y_{22}
$f_{1\min}$	3.66E-3	1.38E-4	4.80E-3	1.89E-4
$f_{2\min}$	3.9E-4	2.40E-4	3.90E-4	2.67E-4
	y_3	y_{33}	y_4	y_{44}
$f_{1\min}$	3.86E-3	1.38E-4	3.66E-4	1.43E-4
$f_{2\min}$	3.97E-4	2.39E-4	3.9E-4	2.4E-4

TABLE 2. The compromise points of NPDNI control law with saturation defined by (51) and (52) after optimization.

	y_1	y_{11}	y_2	y_{22}
f_1	3.82E-3	2.05E-4	4.11E-3	2.85E-4
f_2	4.73E-4	2.95E-4	4.34E-4	3.05E-4
	y_3	y_{33}	y_4	y_{44}
f_1	3.90E-3	2.07E-4	3.82E-3	2.08E-4
f_2	4.53E-4	2.89E-4	4.75E-4	2.89E-4

TABLE 3. The Utopia points of NPPDNI control law with saturation defined by (51) and (52) after optimization.

	y_1	y_{11}	y_2	y_{22}
$f_{1\min}$	3.33E-3	1.20E-4	1.15E-3	1.02E-4
$f_{2\min}$	3.38E-4	2.12E-4	9.24E-5	1.25E-4
	y_3	y_{33}	y_4	y_{44}
$f_{1\min}$	2.28E-3	1.48E-4	1.68E-3	1.02E-4
$f_{2\min}$	3.59E-4	2.36E-4	1.38E-4	1.29E-4

in Figure 8. By comparing (a) and (b), (c) and (d), (e) and (f), (g) and (h), it can be concluded that the trajectory tracking accuracy and the torque output accuracy of the NPPDNI control law with the saturation functions defined by (52) have been improved. The Utopia solutions of NPPDNI control law with saturation defined by (51) and (52) after optimization are shown in Table 3 It can be concluded that the control effect of the NPPDNI control law with saturation function defined by (52) is better than that of the NPPDNI control law with saturation function defined by (51). The errors between the desired output torque and actual output torque with saturation function defined by (52) are less than that with saturation function defined by (51). Compared with the trajectory tracking accuracy with saturation function defined by (51), the trajectory tracking accuracy with saturation function defined by (52) is improved by nearly an order of magnitude. In order to study the robustness of the NPPDNI control law, four groups of compromise solutions shown in TABLE 4 are compared. Taking the importance of the trajectory tracking in practical application, a group (y_{44}) with high trajectory accuracy is selected to study its robustness.

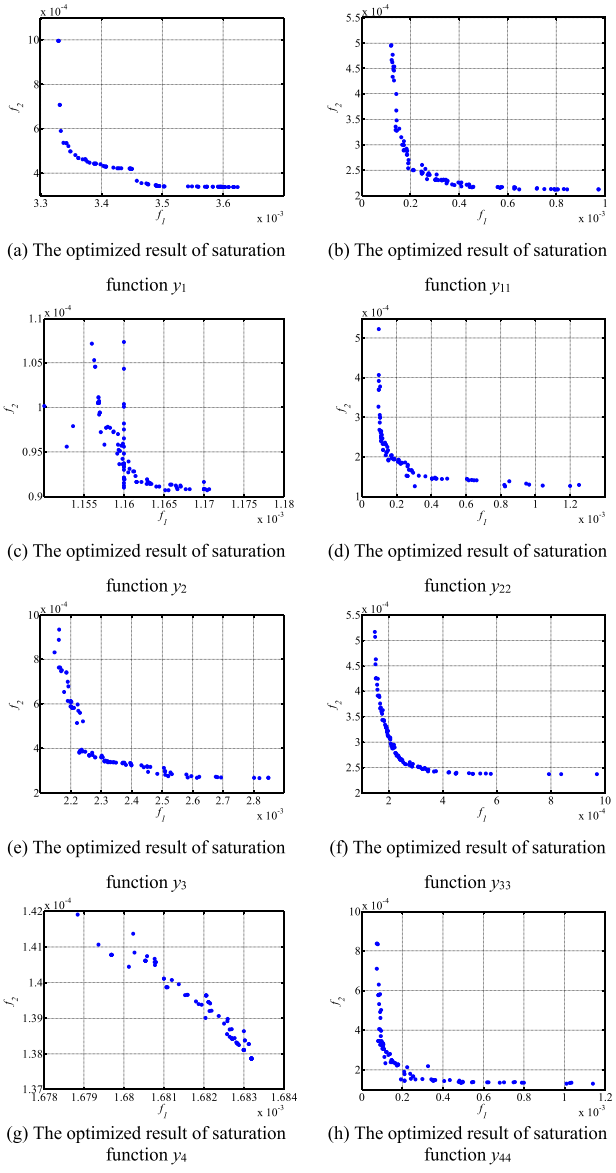

(a) The optimized result of saturation function y_1
(b) The optimized result of saturation function y_{11}
(c) The optimized result of saturation function y_2
(d) The optimized result of saturation function y_{22}
(e) The optimized result of saturation function y_3
(f) The optimized result of saturation function y_{33}
(g) The optimized result of saturation function y_4
(h) The optimized result of saturation function y_{44}

FIGURE 8. The optimized result of the NPPDNI control law.

TABLE 4. The compromise points of NPPDNI control law with saturation defined by (51) and (52) after optimization.

	y_1	y_{11}	y_2	y_{22}
f_1	3.41E-3	1.91E-4	1.15E-3	1.53E-4
f_2	4.31E-4	2.53E-4	9.6E-5	1.91E-4
	y_3	y_{33}	y_4	y_{44}
f_1	2.28E-3	2.09E-4	1.68E-3	1.16E-04
f_2	3.80E-4	2.92E-4	1.40E-4	2.32E-4

V. ROBUSTNESS ANALYSIS OF NONLINEAR PID

In order to compare the robustness of the traditional PID control law, nonlinear PID control law with saturation functions defined by (51), and nonlinear PID control law with saturation function defined by (52), the effects of the model uncertainty, input torque disturbance and noise on the integra-

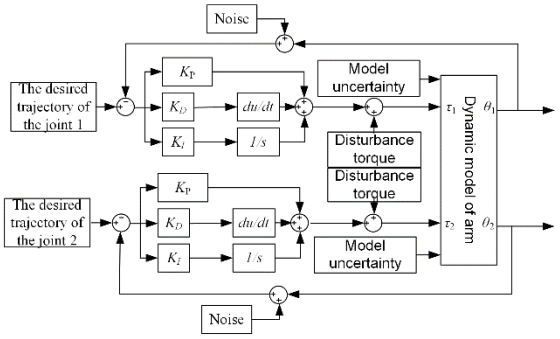

(a) The traditional PID simulation diagram

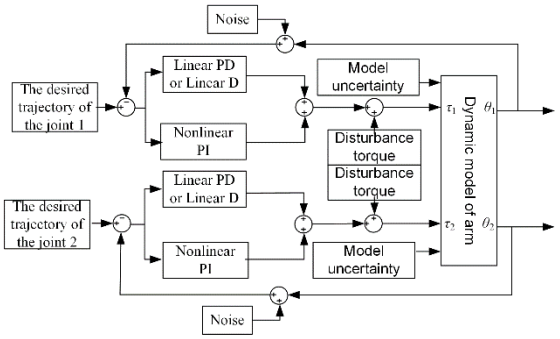

(b) The nonlinear PID simulation diagram

FIGURE 9. **The simulation diagram.**

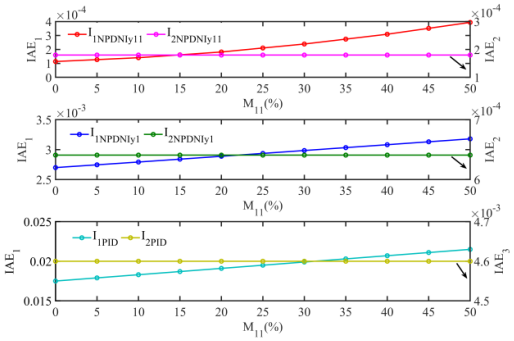

(a) The IAE changes with the mass change of link 1

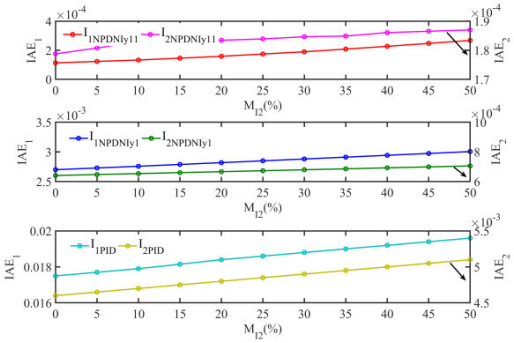

(b) The IAE changes with the mass change of link 2

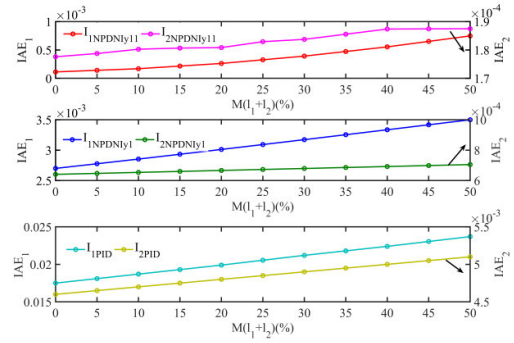

(c) The IAE changes with the mass change of link 1 and link 2 simultaneously

FIGURE 10. **Variation in IAE for mass change of the model.**

tion of the absolute value of the trajectory tracking errors and torque output errors are studied. The simulation schematic diagram is shown in Figure 9.

The model uncertainty is set as: the mass of link 1 and link 2 increases by 5%, 10%, 15%, 20%, 25%, 30%, 35%, 40%, 45%, and 50%, respectively, and the mass of link1 and link 2 increase by 5%, 10%, 15%, 20%, 25%, 30%, 35%, 40%, 45%, and 50% at the same time. The input disturbance torque is set as: the joint 1 and joint 2 are disturbed by 2.5sin(50t), 5sin(50t), 7.5sin(50t), 10sin(50t), 12.5sin(50t), 15sin(50t), 17.5sin(50t), 20sin(50t), 22.5sin (50t), and 25sin(50t) Nm, respectively, and the joint 1 and joint 2 are disturbed by 2.5sin(50t), 5sin(50t), 7.5sin(50t), 10sin(50t), 12.5sin(50t), 15sin(50t), 17.5sin(50t), 20sin (50t), 22.5sin(50t), and 25sin(50t) Nm at the same time. The noise interference is set as: the joint 1 and joint 2 are disturbed by 75dB, 77.5dB, 80dB, 82.5dB, 85dB, 87.5dB, 90dB, 92.5dB, 95dB, 97.5dB and 100dB, respectively, and the joint 1 and joint 2 are disturbed by 75dB, 77.5dB, 80 dB, 82.5dB, 85dB, 87.5dB, 90dB, 92.5dB, 95dB, 97.5dB and 100 dB at the same time.

A. ROBUSTNESS ANALYSIS OF LINEAR D + NONLINEAR PI

As shown in Figure 10 (a), IAE between the desired and actual trajectory of the joint 1 (IAE_1) shows an increasing trend as the mass of link 1 increases, IAE between the desired and actual trajectory of the joint 2 (IAE_2) is not affected by the increase in the mass of link 1, because there is no link 1 mass term in the drive torque model of joint 2, IAE_2 is not affected. As shown in Figure 10 (b), IAE_1 shows an increasing trend as the mass of link 2 increases, because there is link 2 mass term in the drive torque model of joint 1, IAE_2 increases as the mass of link 2 increases. As shown in Figure 10 (c), the IAE_1 and IAE_2 shown an increasing trend as the mass of link 1 and link 2 increase. Compared with Figure 10 (a) and (b), the IAE_1 and IAE_2 are the maximum in Figure 10 (c), because the masses of link 1 and link 2 increase simultaneously, which results in a greater impact on the output torque, the trajectory tracking accuracy is reduced. As shown in Figure 10 (a), (b), and (c), the IEA_1 and IAE_2 of the traditional PID and nonlinear PID with the saturation functions y_1 are larger than them of the nonlinear PID with the saturation functions y_{11}. Because the nonlinear PID control with the saturation functions y_{11} has a strong feedback effect on the error and can quickly compensate the error.

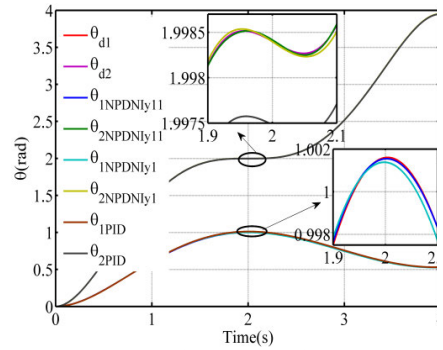

(a) The trajectoy tracking

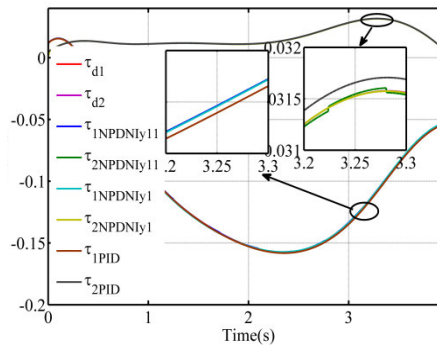

(b) The output torque

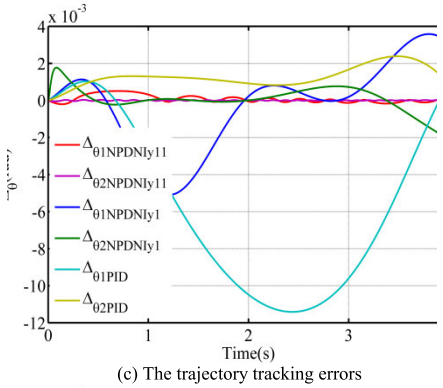

(c) The trajectory tracking errors

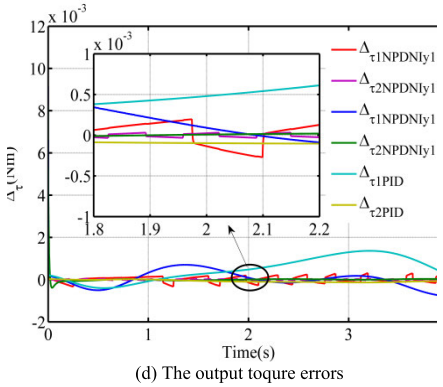

(d) The output toqure errors

FIGURE 11. Performance analysis of control law when the masses of link 1 and 2 increase by 50% simultaneously.

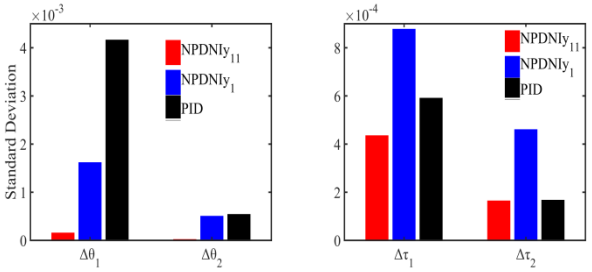

FIGURE 12. The standard deviation of the trajectory tracking error and output torque error.

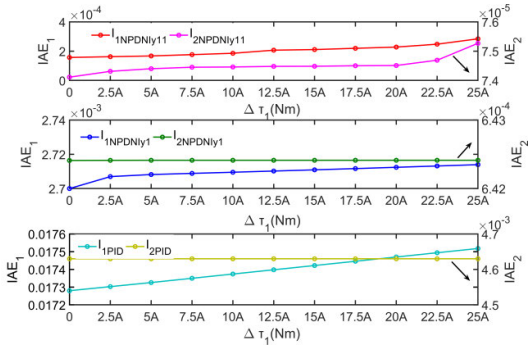

(a) The IAE changes with the input disturbance torque of the joint 1

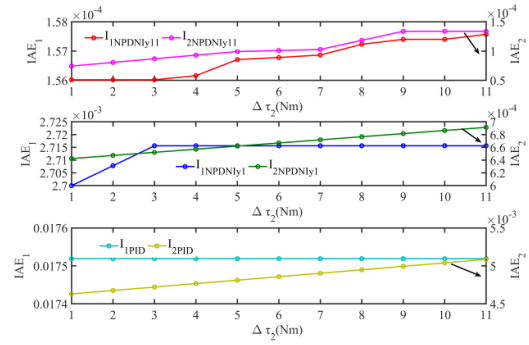

(b) The IAE changes with the input disturbance torque of the joint 2

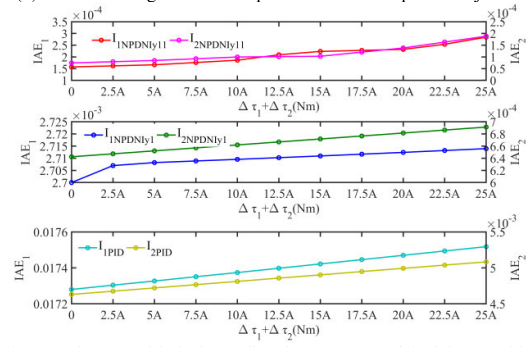

(c) The IAE changes with the input disturbance torque of the joint 1 and joint 2

FIGURE 13. Variation in IAE for input disturbance torque.

As shown in Figure 13 (a), IAE_1 increases as the input disturbance torque of the joint 1 increases. As shown in Figure 13. (b), IAE_2 increases as the input disturbance torque of the joint 2 increases. As shown in Figure 13. (c), IAE_1 and IAE_2 increase as the input disturbance torque of the joint 1 and joint 2 increase simultaneously. Compared with Figure 13 (a) and (b), the IAE_1 and IAE_2 are the maximum, because the input disturbance torque of the joint 1 and

joint 2 increase simultaneously, which results in a greater impact on the output torque, the trajectory tracking accuracy is reduced. As shown in Figure 13 (a), (b), and (c), the IEA_1 and IAE_2 of the nonlinear PID with the saturation functions y_{11} are less than them of the traditional PID and nonlinear PID with the saturation functions y_1. Because the nonlinear PID control with the saturation functions y_{11} has a strong feedback effect on the error and can quickly compensate the error.

The trajectory tracking errors and the output torque errors are shown in Figure 11, when the masses of link 1 and link 2 increase by 50% simultaneously. The trajectory tracking errors and the output torque errors of the joint 1 and joint 2 controlled by the nonlinear PID with the saturation function y_{11} is less than them of the joint 1 and joint 2 controlled by the nonlinear PID with the saturation function y_{11} and the traditional PID, respectively. It indicates that the nonlinear PID with the saturation y_{11} is the most robust to the model uncertainty.

The standard deviation reflects data fluctuation. The smaller the standard deviation is, the smaller the fluctuation of input and motion of the system is, and the system is relatively stable. The standard deviation of the trajectory tracking error and output torque error is shown in Figure 12, the standard deviation of the trajectory tracking error and output torque error of the nonlinear PID with the saturation function y_{11} is the smallest. It indicates that the nonlinear PID with the saturation function y_{11} has high robust to the model uncertainty.

As shown in Figure 13 (a), IAE_1 increases as the input disturbance torque of the joint 1 increases. As shown in Figure 13. (b), IAE_2 increases as the input disturbance torque of the joint 2 increases. As shown in Figure 13. (c), IAE_1 and IAE_2 increase as the input disturbance torque of the joint 1 and joint 2 increase simultaneously. Compared with Figure 13 (a) and (b), the IAE_1 and IAE_2 are the maximum, because the input disturbance torque of the joint 1 and joint 2 increase simultaneously, which results in a greater impact on the output torque, the trajectory tracking accuracy is reduced. As shown in Figure 13 (a), (b), and (c), the IEA_1 and IAE_2 of the nonlinear PID with the saturation functions y_{11} are less than them of the traditional PID and nonlinear PID with the saturation functions y_1. Because the nonlinear PID control with the saturation functions y_{11} has a strong feedback effect on the error and can quickly compensate the error.

The trajectory tracking errors and the output torque errors are shown in Figure 14, when the input disturbance torque of the joint 1 and 2 is 25sin(50t) N·m simultaneously. The trajectory tracking errors and the output torque errors of the joint 1 and joint 2 controlled by the nonlinear PID with the saturation function y_{11} is less than them of the joint 1 and joint 2 controlled by the nonlinear PID with the saturation function y_1 and the traditional PID, respectively.

The standard deviation of the trajectory tracking error and output torque error is shown in Figure 15, the standard deviation of the trajectory tracking error and output torque error of the nonlinear PID with the saturation function y_{11} is the smallest. It indicates that the nonlinear PID with the saturation function y_{11} has high robust to the input disturbance torque.

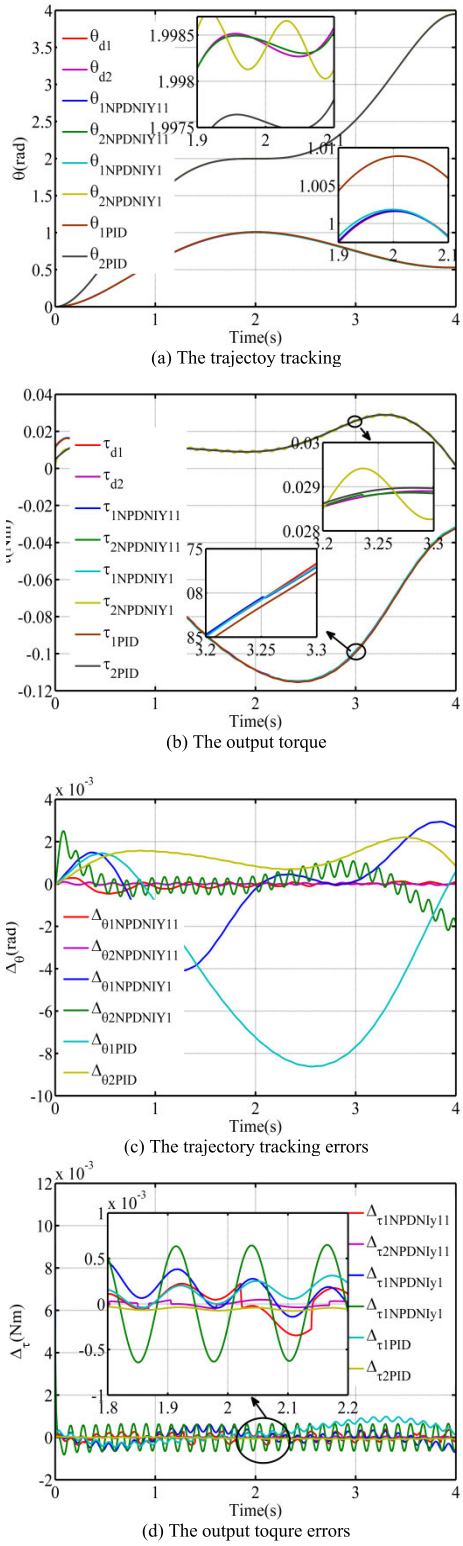

FIGURE 14. Performance analysis of control law when the input disturbance torque of the joint 1 and 2 is 25sin(50t) Nm.

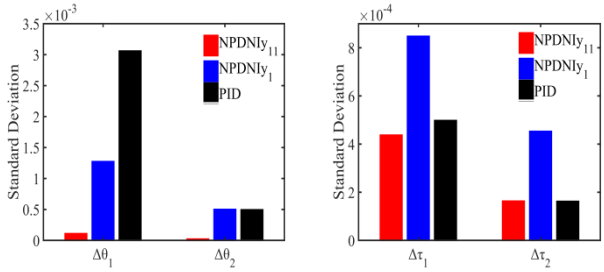

FIGURE 15. The standard deviation of the trajectory tracking error and output torque error.

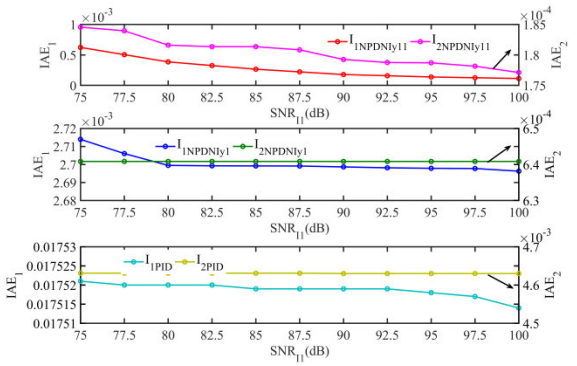

(a) The IAE changes with the SNR change of the joint 1

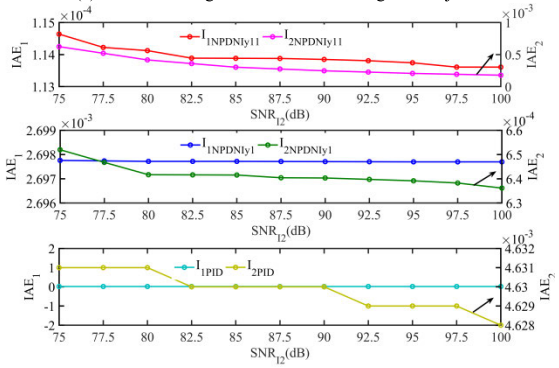

(b) The IAE changes with the SNR change of the joint 2

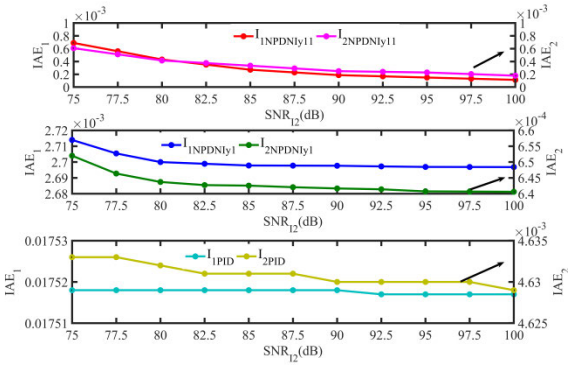

(c) The IAE changes with the SNR change of the joint 1 and joint 2 simultaneously

FIGURE 16. Variation in IAE for SNR change.

As shown in Figure 16 (a), IAE_1 decreases as the input noise disturbance of the joint 1 reduces (It means signal noise ratio (SNR) increases). As shown in Figure 16 (b), IAE_2 decreases as the input noise disturbance of the joint 2 reduces. As shown in Figure 16 (c), IAE_1 and IAE_2 decrease as the input noise disturbance of the joint 1 and joint 2 reduces simultaneously. Compared with Figure 16 (a) and (b), the IAE_1 and IAE_2 are the maximum, because the input noise disturbance of the joint 1 and joint 2 increase simultaneously, which results in a greater impact on the output torque, the trajectory tracking accuracy is reduced. As shown in Figure 16 (a), (b), and (c), the IEA_1 and IAE_2 of the nonlinear PID with the saturation functions y_{11} are less than them of the traditional PID and nonlinear PID with the saturation functions y_1. Because the nonlinear PID control with the saturation functions y_{11} has strong feedback effect on the error and can quickly compensate the error.

The trajectory tracking errors and the output torque errors are shown in Figure 17, when the input noise disturbance of the joint 1 and 2 is 75dB simultaneously. The trajectory tracking errors and the output torque errors of the joint 1 and joint 2 controlled by the nonlinear PID with the saturation function y_{11} is less than them of the joint 1 and joint 2 controlled by the nonlinear PID with the saturation function y_1 and the traditional PID, respectively. It indicates that the nonlinear PID with the saturation y_{11} is the most robust to the noise disturbance.

The standard deviation of the trajectory tracking error and output torque error is shown in Figure 18, the standard deviation of the trajectory tracking error and output torque error of the nonlinear PID with the saturation function y_{11} is the smallest. It indicates that the nonlinear PID with the saturation function y_{11} has high robust to the noise disturbance.

B. ROBUSTNESS ANALYSIS OF LINEAR PD + NONLINEAR PI

As shown in Figure 19 (a), IAE between the desired and actual trajectory of the joint 1 (IAE_1) shows an increasing trend as the mass of link 1 increases, IAE between the desired and actual trajectory of the joint 2 (IAE_2) is not affected by the increase in the mass of link 1, because there is no link 1 mass term in the drive torque model of link 2, IAE_2 is not affected. As shown in Figure 19 (b), IAE_1 shows an increasing trend as the mass of link 2 increases, because there is link 2 mass term in the drive torque model of link 1, IAE_2 increases as the mass of link 2 increases. As shown in Figure 19 (c), the IAE_1 and IAE_2 shown an increasing trend as the mass of link 1 and link 2. Compared with Figure 19 (a) and (b), the IAE_1 and IAE_2 are the maximum, because the masses of link 1 and link 2 increase simultaneously, which results in a greater impact on the output torque, the trajectory tracking accuracy is reduced. As shown in Figure 19 (a), (b), and (c), the IEA_1 and IEA_2 of the traditional PID and nonlinear PID with the saturation functions y_4 are larger than them of the nonlinear PID with the saturation functions y_{44}. Because the nonlinear PID control with the saturation functions y_{44} has a strong feedback effect on the error and can quickly compensate the error.

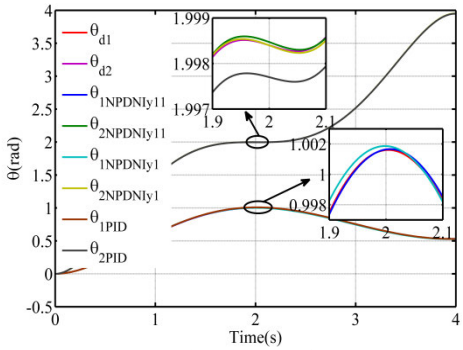

(a) The trajectoy tracking

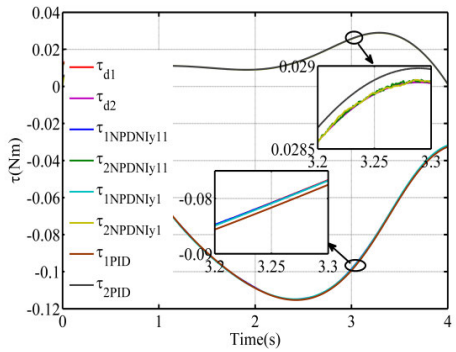

(b) The output torque

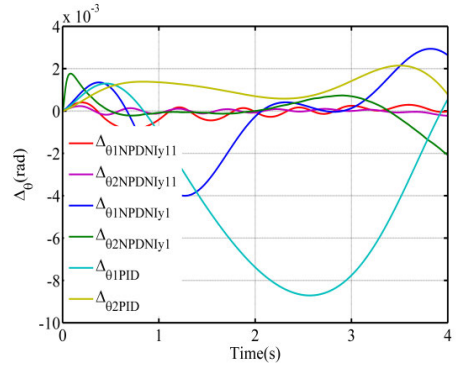

(c) The trajectory tracking errors

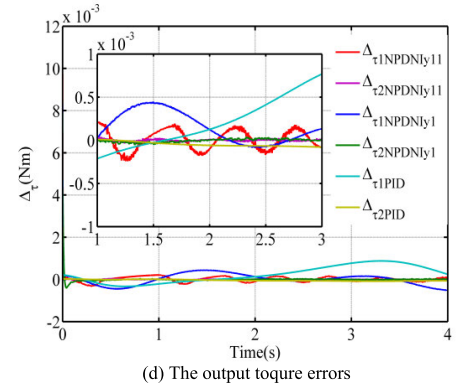

(d) The output toqure errors

FIGURE 17. Performance analysis of control law when the SNR of the joint 1 and joint 2 is 75dB.

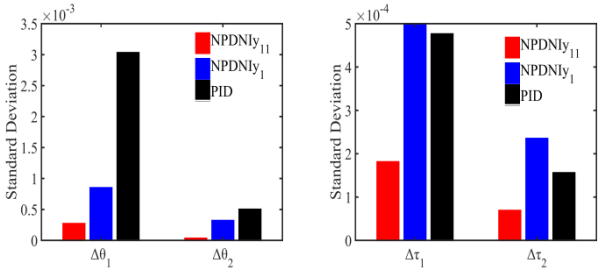

FIGURE 18. The standard deviation of the trajectory tracking error and output torque error.

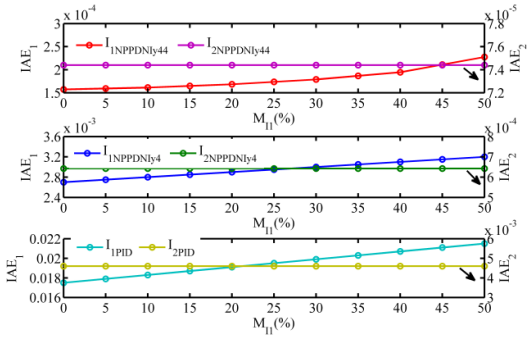

(a) The IAE changes with the mass change of link 1

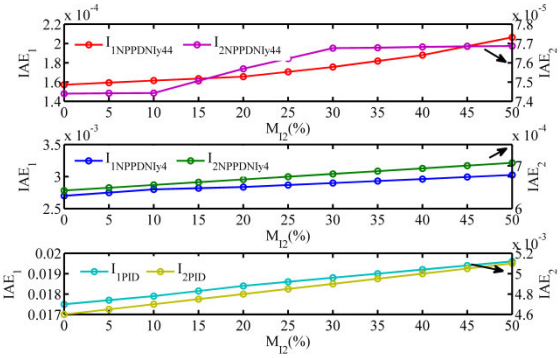

(b) The IAE changes with the mass change of link 2

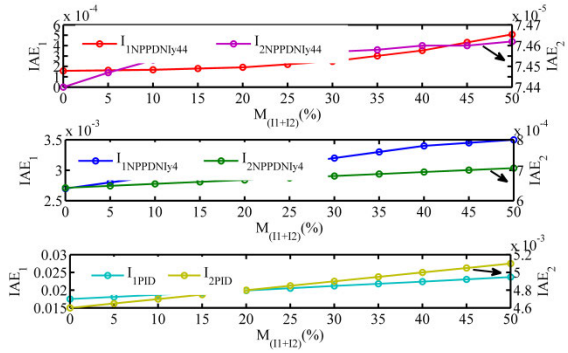

(c) The IAE changes with the mass change of link 1 and link 2 simultaneously

FIGURE 19. Variation in IAE for mass change of the model.

The trajectory tracking errors and the output torque errors are shown in Figure 20, when the masses of link 1 and link 2 increases by 50% simultaneously. The trajectory tracking errors and the output torque errors of the joint 1 and joint 2 controlled by the nonlinear PID with the saturation function y_{44} is less than them of the joint 1 and joint 2 controlled by the nonlinear PID with the saturation function y_4 and the

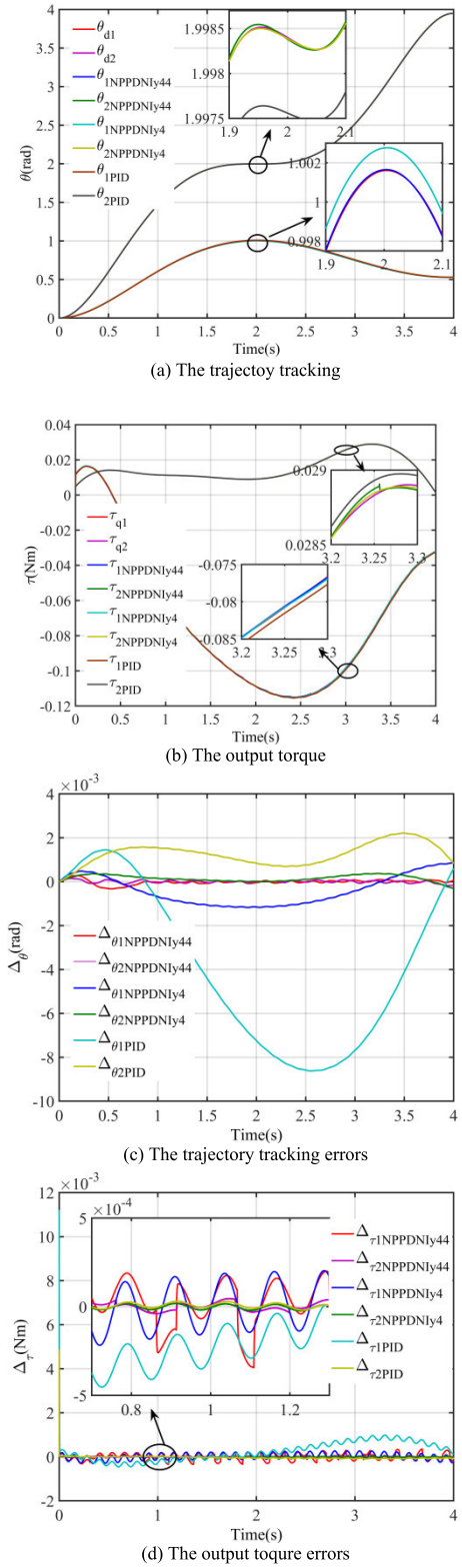

(a) The trajectoy tracking
(b) The output torque
(c) The trajectory tracking errors
(d) The output toqure errors

FIGURE 20. Performance analysis of control law when the masses of link 1 and 2 increase by 50% simultanously.

traditional PID, respectively. It indicates that the nonlinear PID with the saturation y_{44} is the most robust to the model uncertainty.

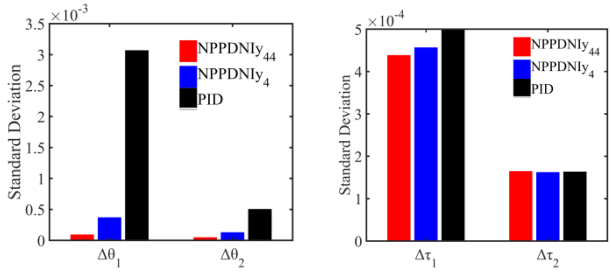

FIGURE 21. The standard deviation of the trajectory tracking error and output torque error.

The standard deviation of the trajectory tracking error and output torque error is shown in Figure 21, the standard deviation of the trajectory tracking error and output torque error of the nonlinear PID with the saturation function y_{44} is the smallest. It indicates that the nonlinear PID with the saturation function y_{44} has high robust to the noise disturbance.

As shown in Figure 22. (a), IAE_1 increases as the input disturbance torque of the joint 1 increases. As shown in Figure 22. (b), IAE_2 increases as the input disturbance torque of the joint 2 increases. As shown in Figure 22. (c), IAE_1 and IAE_2 increase as the input disturbance torque of the joint 1 and joint 2 increase simultaneously. Compared with Figure 22 (a) and (b), the IAE_1 and IAE_2 are the maximum, because the input disturbance torque of the joint 1 and joint 2 increase simultaneously, which results in a greater impact on the output torque, the trajectory tracking accuracy is reduced. As shown in Figure 22 (a), (b), and (c), the IAE_1 and IAE_2 of the nonlinear PID with the saturation functions y_{44} are less than them of the traditional PID and nonlinear PID with the saturation functions y_4. Because the nonlinear PID control with the saturation functions y_{44} has a strong feedback effect on the error and can quickly compensate the error.

The trajectory tracking errors and the output torque errors are shown in Figure 23, when the input disturbance torque of the joint 1 and 2 is 25sin(50t) N·m simultaneously. The trajectory tracking errors and the output torque errors of the joint 1 and joint 2 controlled by the nonlinear PID with the saturation function y_{44} are less than them of the joint 1 and joint 2 controlled by the nonlinear PID with the saturation function y_4 and the traditional PID, respectively. It indicates that the nonlinear PID with the saturation y_{44} is the most robust to the input disturbance torque.

The standard deviation of the trajectory tracking error and output torque error is shown in Figure 24, the standard deviation of the trajectory tracking error and output torque error of the nonlinear PID with the saturation function y_{44} is the smallest. It indicates that the nonlinear PID with the saturation y_{44} has high robust to the input disturbance torque.

As shown in Figure 25 (a), IAE_1 decreases as the input noise disturbance of the joint 1 reduces (It means signal noise ratio (SNR) increases). As shown in Figure 25 (b), IAE_2 decreases as the input noise disturbance of the joint 2 reduces. As shown in Figure 25 (c), IAE_1 and IAE_2

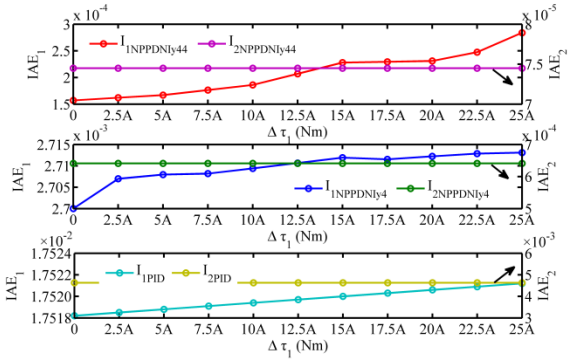

(a) The IAE changes with the input disturbance torque of the joint 1

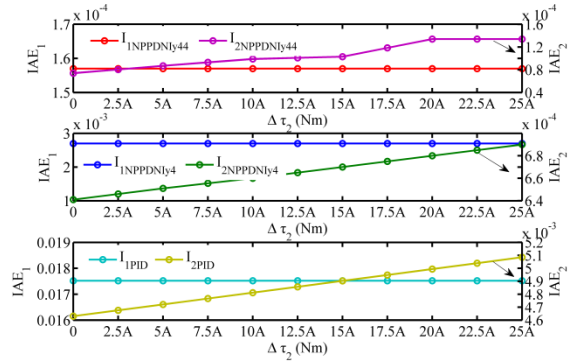

(b) The IAE changes with the input disturbance torque of the joint 2

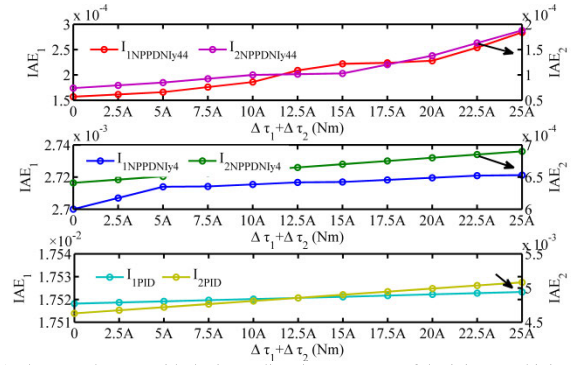

(c) The IAE changes with the input disturbance torque of the joint 1 and joint 2 simultaneously A= sin(50t)

FIGURE 22. Variation in IAE for input disturbance torque.

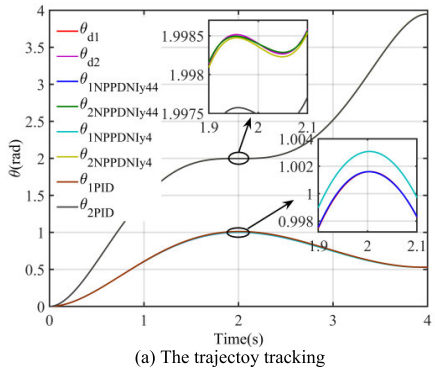

(a) The trajectoy tracking

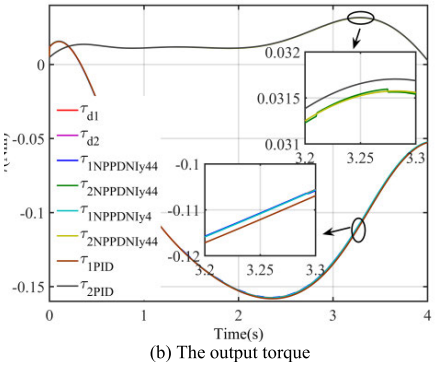

(b) The output torque

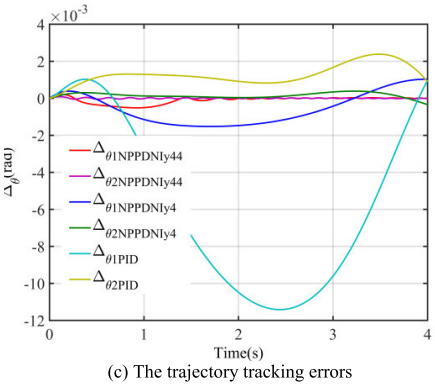

(c) The trajectory tracking errors

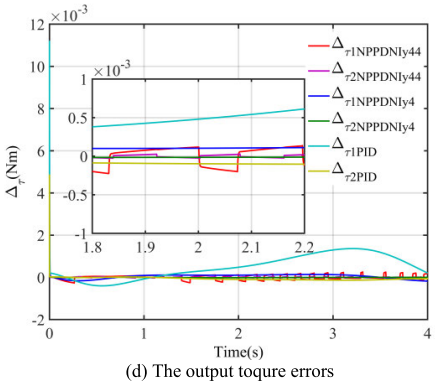

(d) The output toqure errors

FIGURE 23. Performance analysis of control law when the input disturbance torque of the joint 1 and 2 is 25sin(50t) Nm.

decrease as the input noise disturbance of the joint 1 and joint 2 reduces simultaneously. Compared with Figure 25 (a) and (b), the IAE_1 and IAE_2 are the maximum, because the input noise disturbance of the joint 1 and joint 2 increase simultaneously, which results in a greater impact on the output torque, the trajectory tracking accuracy is reduced. As shown in Figure 25 (a), (b), and (c), the IAE_1 and IAE_2 of the nonlinear PID with the saturation functions y_{44} are less than them of the traditional PID and nonlinear PID with the saturation functions y_4. Because the nonlinear PID control with the saturation functions y_{44} has a strong feedback effect on the error and can quickly compensate the error.

The trajectory tracking errors and the output torque errors are shown in Figure 26, when the input noise disturbance of the joint 1 and 2 is 75dB simultaneously. The trajectory tracking errors and the output torque errors of the joint 1 and joint 2 controlled by the nonlinear PID with the saturation function y_{44} is less than them of the joint 1 and joint 2 controlled

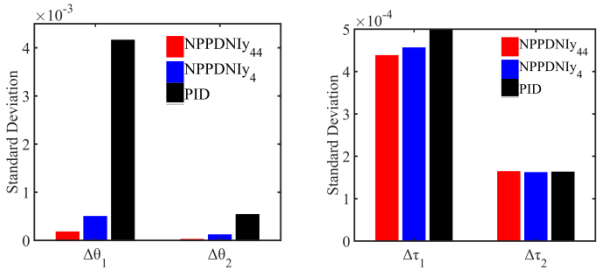

FIGURE 24. The standard deviation of the trajectory tracking error and output torque error.

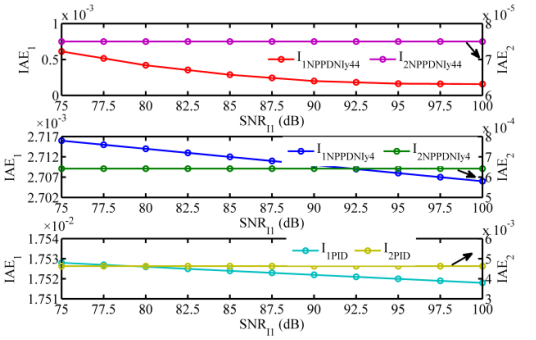

(a) The IAE changes with the SNR change of the joint 1

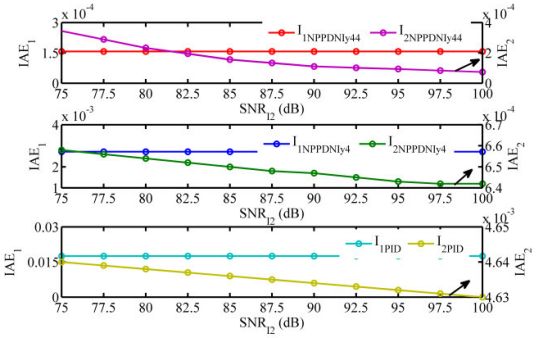

(b) The IAE changes with the SNR change of the joint 2

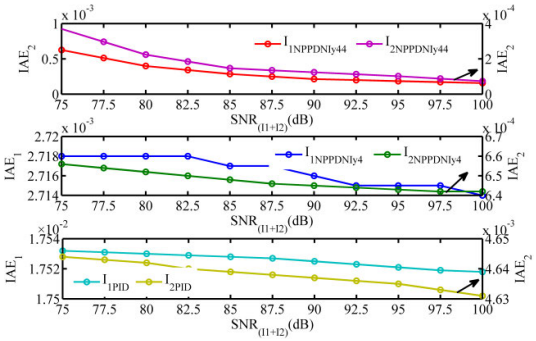

(c) The IAE changes with the SNR change of the joint 1 and joint 2 simultaneously

FIGURE 25. Variation in IAE for SNR change.

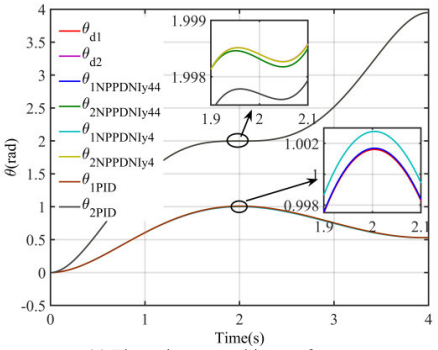

(a) The trajectoy tracking performance

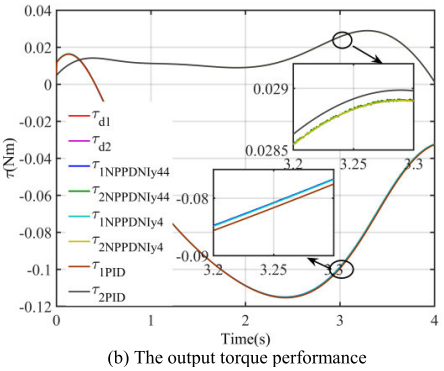

(b) The output torque performance

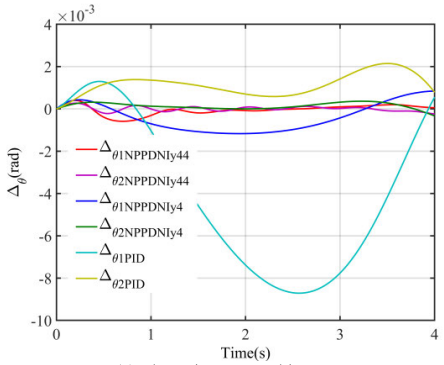

(c) The trajectory tracking errors

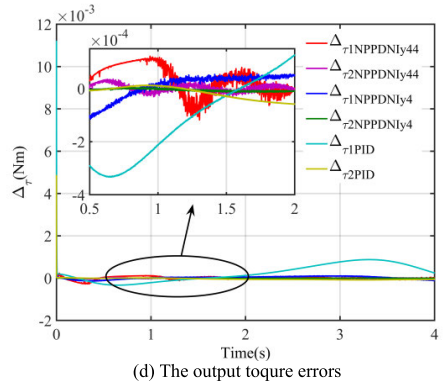

(d) The output toqure errors

FIGURE 26. Performance analysis of control law when the SNR of the joint 1 and joint 2 is 75dB.

by the nonlinear PID with the saturation function y_4 and the traditional PID, respectively. It indicates that the nonlinear PID with the saturation y_{44} is the most robust to the noise disturbance.

The standard deviation of the trajectory tracking error and output torque error is shown in Figure 27, the standard deviation of the trajectory tracking error and output torque error

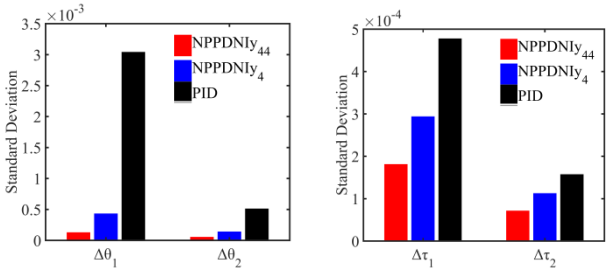

FIGURE 27. The standard deviation of the trajectory tracking error and output torque error.

of the nonlinear PID with the saturation function y_{44} is the smallest. It indicates that the nonlinear PID with the saturation function y_{44} has high robust to the noise disturbance.

Based on the above analysis, linear D + nonlinear PI with the new generalized saturation function and linear PD + nolinear PI with the new generalized saturation function have higher robust to the model uncertainty, input disturbance torque and noise disturbance than the traditional PID, linear D + nonlinear PI with the common saturation function and linear PD + nolinear PI the common saturation function. Because the new generalized saturation function has a strong feedback effect on the error and can quickly compensate the error.

VI. CONCLUSION

First, a new generalized saturation function was proposed, which had strong reaction near the equilibrium point and can make the control converge to the equilibrium point quickly. Second, the proposed generalized saturation function was applied in linear D + nonlinear PI control law and in linear PD + nonlinear PI control law, the corresponding GAS conditions of the above two control laws were proved using Lyapunov's method and LaSalle's invariance principle. Third, the parameters tuning models of the above two control laws with the proposed saturation function and the common saturation function were built, the time integration of the absolute value of position tracking error and time integration of the absolute value of input torque error were chosen as the objective functions, the GAS conditions and the rate driving torque of each motor are regarded as the constraint conditions. The control laws with the proposed saturation function had high position tracking accuracy and torque output to prove the excellent characteristics of the proposed saturation function. Last, Robustness to the model uncertainty, input disturbance torque and noise disturbance of the tradition PID control law, the above two control laws with the common saturation functions, and the above two control laws with the proposed saturation functions was studied, the results shown that control laws with the proposed saturation functions had high robustness.

REFERENCES

[1] A. Visioli and G. Legnani, "On the trajectory tracking control of industrial SCARA robot manipulators," *IEEE Trans. Ind. Electron.*, vol. 49, no. 1, pp. 224–232, Aug. 2002.
[2] J. Alvarez-Ramirez, R. Kelly, and I. Cervantes, "Semiglobal stability of saturated linear PID control for robot manipulators," *Automatica*, vol. 39, no. 6, pp. 989–995, Jun. 2003.
[3] J. Alvarez-Ramirez, V. Santibanez, and R. Campa, "Stability of robot manipulators under saturated PID compensation," *IEEE Trans. Control Syst. Technol.*, vol. 16, no. 6, pp. 1333–1341, Nov. 2008.
[4] R. Ortega, A. Loria, and R. Kelly, "A semiglobally stable output feedback PI^2D regulator for robot manipulators," *IEEE Trans. Autom. Control*, vol. 40, no. 8, pp. 1432–1436, Aug. 1995.
[5] B.-S. Liu and F.-C. Lin, "A semiglobally stable PD-I(PD) regulator for robot manipulators," in *Proc. Int. Conf. Measuring Technol. Mechatronics Autom.*, New York, NY, USA, 2009, pp. 763–766.
[6] R. Kelly, "Global positioning of robot manipulators via PD control plus a class of nonlinear integral actions," *IEEE Trans. Autom. Control*, vol. 43, no. 7, pp. 934–938, Jul. 1998.
[7] R. Gorez, "Globally stable PID-like control of mechanical systems," *Syst. Control Lett.*, vol. 38, no. 1, pp. 61–72, Sep. 1999.
[8] M. Mendoza, A. Zavala-Río, V. Santibáñez, and F. Reyes, "A generalised PID-type control scheme with simple tuning for the global regulation of robot manipulators with constrained inputs," *Int. J. Control*, vol. 88, no. 10, pp. 1995–2012, Apr. 2015.
[9] M. Mendoza, A. Zavala-Río, V. Santibáñez, and F. Reyes, "Output-feedback proportional–integral–derivative-type control with simple tuning for the global regulation of robot manipulators with input constraints," *IET Control Theory Appl.*, vol. 9, no. 14, pp. 2097–2106, Sep. 2015.
[10] V. Santibañez, K. Camarillo, J. Moreno-Valenzuela, and R. Campa, "A practical PID regulator with bounded torques for robot manipulators," *Int. J. Control, Autom. Syst.*, vol. 8, no. 3, pp. 544–555, Jun. 2010.
[11] A. Zavala-Rio and V. Santibanez, "A natural saturating extension of the PD-with-desired-gravity-compensation control law for robot manipulators with bounded inputs," *IEEE Trans. Robot.*, vol. 23, no. 2, pp. 386–391, Apr. 2007.
[12] A. Zavala-Rio and V. Santibanez, "Simple extensions of the PD-with-gravity-compensation control law for robot manipulators with bounded inputs," *IEEE Trans. Control Syst. Technol.*, vol. 14, no. 5, pp. 958–965, Sep. 2006.
[13] A. Zavalario, M. Mendoza, V. Santibanez, and F. Reyes, "Output-feedback proportional-integral-derivative -type control with multiple saturating structure for the global stabilization of robot manipulators with bounded inputs," *Int. J. Adv. Robot. Syst.*, vol. 13, no. 5, pp. 1–12, Jul. 2016.
[14] A. Salinas, J. Moreno-Valenzuela, and R. Kelly, "A family of nonlinear PID-like regulators for a class of torque-driven robot manipulators equipped with torque-constrained actuators," *Adv. Mech. Eng.*, vol. 8, no. 2, pp. 1–12, Feb. 2016.
[15] A. Yarza, V. Santibanez, and J. Moreno-Valenzuela, "Global asymptotic stability of the classical PID controller by considering saturation effects in industrial robots," *Int. J. Adv. Robot. Syst.*, vol. 8, no. 4, pp. 34–42, Sep. 2011.
[16] B. S. Liu, F. C. Lin, and B. L. Tian, "A set of globally stable N-PID regulators for robotic manipulators," *Engineering*, vol. 2, no. 2, pp. 118–123, 2010.
[17] Y. Su, P. C. Muller, and C. Zheng, "Global asymptotic saturated PID control for robot manipulators," *IEEE Trans. Control Syst. Technol.*, vol. 18, no. 6, pp. 1280–1288, Nov. 2010.
[18] N. J. Killingsworth and M. Krstić, "PID tuning using extremum seeking: Online, model-free performance optimization," *IEEE Control Syst. Mag.*, vol. 26, no. 1, pp. 70–79, Feb. 2006.
[19] H.-B. Duan, D.-B. Wang, and X.-F. Yu, "Novel approach to nonlinear PID parameter optimization using ant colony optimization algorithm," *J. Bionic Eng.*, vol. 3, no. 2, pp. 73–78, Jun. 2006.
[20] K. Li, "PID tuning for optimal closed-loop performance with specified gain and phase margins," *IEEE Trans. Control Syst. Technol.*, vol. 21, no. 3, pp. 1024–1030, May 2013.
[21] W. Chang, "A multi-crossover genetic approach to multivariable PID controllers tuning," *Expert Syst. Appl.*, vol. 33, no. 3, pp. 620–626, Oct. 2007.
[22] S. Panda, "Multi-objective PID controller tuning for a FACTS-based damping stabilizer using non-dominated sorting genetic algorithm-II," *Int. J. Electr. Power Energy Syst.*, vol. 33, no. 7, pp. 1296–1308, Sep. 2011.
[23] J. Han, P. Wang, and X. Yang, "Tuning of PID controller based on fruit fly optimization algorithm," in *Proc. IEEE Int. Conf. Mechatronics Autom.*, New York, NY, USA, Aug. 2012, pp. 409–413.
[24] J. Sun, H. Zhou, X. Ma, and Z. Ju, "Study on PID tuning strategy based on dynamic stiffness for radial active magnetic bearing," *ISA Trans.*, vol. 80, pp. 458–474, Sep. 2018.

[25] M. A. Khodja, M. Tadjine, M. S. Boucherit, and M. Benzaoui, "Tuning PID attitude stabilization of a quadrotor using particle swarm optimization (experimental)," *Int. J. Simul. Multidisc. Des. Optim.*, vol. 8, no. A8, pp. 1–9, Jan. 2017.
[26] A. Leva, A. V. Papadopoulos, S. Seva, and C. Cimino, "Explicit model-based real PID tuning for efficient load disturbance rejection," *Ind. Eng. Chem. Res.*, vol. 58, no. 51, pp. 1–40, Dec. 2019.
[27] M. S. Can and O. F. Ozguven, "PID tuning with neutrosophic similarity measure," *Int. J. Fuzzy Syst.*, vol. 19, no. 2, pp. 489–503, Apr. 2017.
[28] J. Garrido, M. Ruz, F. Morilla, and F. Vázquez, "Interactive tool for frequency domain tuning of PID controllers," *Processes*, vol. 6, no. 10, p. 197, Oct. 2018.
[29] M. Kang, J. Cheong, H. M. Do, Y. Son, and S.-I. Niculescu, "A practical iterative PID tuning method for mechanical systems using parameter chart," *Int. J. Syst. Sci.*, vol. 48, no. 13, pp. 2887–2900, Jul. 2017.
[30] A. R. Teel, "Global stabilization and restricted tracking for multiple integrators with bounded controls," *Syst. Control Lett.*, vol. 18, no. 3, pp. 165–171, Mar. 1992.
[31] R. Kelly, V. Santibanez, and A. Loria, *Control of Robot Manipulators in Joint Space*. London, U.K.: Springer-Verlag, 2005.
[32] G. Niu, B. Pan, Y. Fu, and C. Qu, "Development of a new medical robot system for minimally invasive surgery," *IEEE Access*, vol. 8, pp. 144136–144155, Aug. 2020.
[33] G. J. Liu, "Analysis and structural parameter optimization of 6-DOF motion simulation platform," Ph.D. dissertation, School Mech. Eng., Harbin Inst. Technol., Harbin, China, 2014.
[34] H. V. H. Ayala and L. dos Santos Coelho, "Tuning of PID controller based on a multiobjective genetic algorithm applied to a robotic manipulator," *Expert Syst. Appl.*, vol. 39, no. 10, pp. 8968–8974, Aug. 2012.
[35] H. Ghassemi and H. Zakerdoost, "Ship hull–propeller system optimization based on the multi-objective evolutionary algorithm," *Proc. Inst. Mech. Eng., C, J. Mech. Eng. Sci.*, vol. 231, no. 1, pp. 1–18, Nov. 2015.

GUOJUN NIU received the M.S. degree in mechanical design and theory, and the Ph.D. degree in mechatronics engineering from the Harbin Institute of Technology, China, in 2011 and 2017, respectively. He is currently a Lecturer with the School of Mechanical Engineering and Automation, Zhejiang Sci-Tech University, China. His research interests include robotic optimization design, control and force estimation, and force feedback.

CUICUI QU received the M.S. degree in mechanical manufacture and automation from the Harbin University of Science and Technology, China, in 2013. She is currently an Engineer with Hangzhou SIASUN Robot and Automation Company Ltd., China. Her research interests include robotic design and automatic production.